Commensalism and syntrophy in the chemostat: a unifying graphical approach

Tewfik Sari

Commensalism and syntrophy in the chemostat: a unifying graphical approach[*]

Tewfik Sari [†]

March 21, 2024

Abstract

The aim of this paper is to show that Tilman's graphical method for the study of competition between two species for two resources can be advantageously used also for the study of commensalism or syntrophy models, where a first species produces the substrate necessary for the growth of the second species. The growth functions of the species considered are general and include both inhibition by the other substrate and inhibition by the species' limiting substrate, when it is at a high concentration. Because of their importance in microbial ecology, models of commensalism and syntrophy, with or without self-inhibition, have been the subject of numerous studies in the literature. We obtain a unified presentation of a large number of these results from the literature. The mathematical model considered is a differential system in four dimensions. We give a new result of local stability of the positive equilibrium which has only been obtained in the literature in the case where the removal rates of the species are identical to the dilution rate and the study of stability can be reduced to that of a system in two dimensions. We describe the operating diagram of the system: this is the bifurcation diagram which gives the asymptotic behavior of the system when the operating parameters are varied, i.e. the dilution rate and the substrate inlet concentrations.
Keywords Commensalim, Syntrophy, Stability, Operating diagram, Bifurcation analysis
Mathematics Subject Classification: 37N25, 92D25, 34D23, 34D15

Contents

[*]This work was presented as part of the CIMPA summer school Digital Green: mathematical biology and theoretical ecology.
[†]Univ Montpellier, INRAE, Institut Agro, Montpellier, France. tewfik.sari@inrae.fr

1 Introduction

The study of interactions within microbial ecological communities is one of the most important issues in microbial ecology [17, 22, 25, 46]. An interaction has an impact (neutral, beneficial or detrimental) on the partner microorganisms involved. Commensalism and syntrophy are among the interactions that benefit the species. A commensalistic association is a relationship in which one microbe derives benefits from the other, while the other microbe is not affected (neither detrimental nor beneficial) by the association. A food chain can be considered a commensal interaction, when the second organism in the food chain lives off the waste products of the first, which in turn is unaffected by the interaction [36, 47]. In a syntrophic association, both organisms benefit from the presence of the other. A food chain can be seen as a syntrophic interaction when the first organism in the food chain is inhibited by the accumulation of its own waste in the environment. This inhibition is diminished by the second organism, which uses the wastes of the first one as a food source [11, 28, 18, 39, 40, 59, 60].

The aim of this work is the present a unified graphical approach of the models of two species having a commensalistic or a syntrophic relationship. Our objective is threefold. First, we show that the graphical concepts introduced by Tilman to study patterns of competition allow us to study these patterns of commensalism and syntrophy in a unified graphical way. Second, we determine the operating diagram of the model, thus obtaining an extension of all the results on the operating diagrams of the literature. Thirdly to consider the case including mortality, which has not been always addressed in previous studies.

Concerning the first objective, we show that the concepts and graphical methods of Tilman [50, 51], complemented by Ballyk and Wolkowicz [3], to determine the outcome of competition between two species for two resources are very useful to understand the condition of existence and stability of the equilibria of commensalistic and syntrophic models. Although these systems are not competitive systems, it appears that the concepts introduced in [3, 50, 51] permit a unifying graphical approach of their study.

Concerning the second objective, we recall that the operating diagram has the operating parameters as its coordinates and the various regions defined within it correspond to qualitatively different asymptotic behaviors. Our model has three operating parameters that are the input concentrations of substrate and the dilution rate D. These parameters are control parameters since they are under the control of the experimenter. Apart from these three parameters, that can vary, all other parameters have biological meaning and are fitted using experimental data from ecological and/or biological observations of organisms and substrates. Therefore the operating diagram is the bifurcation diagram that shows how the system behaves when we vary the control parameters. The importance of the operating diagram for bioreactors was emphasized in [35]. Although this diagram was not considered in the classic monograph on the chemostat [45], its importance was mentioned by Smith and Waltman, who stated that the operating diagram is probably the most useful answer for discussing the behavior of the model in relation to the parameters, [45, p. 252]. The operating diagram is constructed in the recent book on the mathematical theory of the chemostat [23]. It is often constructed both in the biological literature [26, 30, 55, 60] and in the mathematical literature, in the study of anaerobic digestion [10, 27, 57, 58], commensalistic and syntrophic systems [15, 20, 37, 38, 40], microbial food-webs [34, 41, 55], inhibition [4, 16], chemostats in series [12, 13, 14] and density-dependent models [1, 21, 32, 33].

Concerning the third objective, when there is no mortality, by using the theory of asymptotically autonomous systems, we can reduce the study to that of a model in dimension two, so that the study of the stability is easy. In the general case, this reduction cannot be made and the Routh Hurwitz conditions must be used to determine whether the equilibrium is stable or not.

This paper is organized as follows: in Section 2, we present the mathematical model and give the assumptions made on the growth functions. In Section 3 we describe the Tilman's graphical method and we show how the existence and stability condition of the equilibria of the model can be easily read on the position of the projections of equilibria into the *feasible set*. We also construct in this section the operating diagram of the model. In Section 4 we show that the graphical method also applies in the case where the species can be inhibited by their limiting substrate. Finally some conclusions are drawn in Section 5. Some complements on the operating diagrams are given in Appendix A. Global asymptotic stability results are given in Appendix B and bifurcations diagrams with respect to one operating parameters are shown in Appendix C. The technical proofs are reported in Appendix D. In Appendix E, we propose a review of the results of the literature on commensalism and syntrophy.

2 Mathematical model

We consider the two-species system modelled by:

$$\begin{array}{rcl} \dot{S}_1 & = & D\left(S_1^{in} - S_1\right) - k_1\mu_1\left(S_1, S_2\right)X_1, \\ \dot{X}_1 & = & \left(\mu_1\left(S_1, S_2\right) - D_1\right)X_1, \\ \dot{S}_2 & = & D\left(S_2^{in} - S_2\right) + k_3\mu_1\left(S_1, S_2\right)X_1 - k_2\mu_2\left(S_1, S_2\right)X_2, \\ \dot{X}_2 & = & \left(\mu_2\left(S_1, S_2\right) - D_2\right)X_2, \end{array} \tag{2.1}$$

where X_i, $i = 1, 2$, represents the concentration of species i; S_j, $j = 1, 2$, is the concentration of chemical j and S_j^{in} its inlet concentration; k_i, $i = 1, 2, 3$ are yield factors, referring to the amount of chemical that is produced or consumed by the growth of a unit amount of the biomass of microbial species; D_i, $i = 1, 2$ represents the disappearance rates of species i and are modelled by:

$$D_i = \alpha_i D + a_i, \tag{2.2}$$

where $D = 1/HRT$ is the dilution rate, where HRT is the hydraulic retention time; the non-negative death (or decay) rate parameters a_1 and a_2 are taken into consideration; the coefficient $\alpha_i \in [0,1]$, $i = 1,2$, represents the biomass proportion that leaves the bioreactor. This coefficient models the decoupling between solids and hydraulic residence tim [37, 38].

Well-mixed continuous bioreactors (i.e. chemostats) for the culture of multiple species are modelled with the commonly used Monod-type kinetics. For example, in [17], the growth rates of the two species, μ_i, are modelled by multiplying substrate limitation terms described as Monod kinetics and inhibition terms, as follows:

$$\mu_1(S_1,S_2) = \frac{m_1 S_1}{K_1+S_1}\frac{1}{1+L_1 S_2}, \qquad \mu_2(S_1,S_2) = \frac{m_2 S_2}{K_2+S_2}\frac{1}{1+L_2 S_1}, \tag{2.3}$$

where, m_i is the maximum growth rate, K_i is the half-velocity constant, and L_i quantifies the strength of inhibition of substrate S_j, $j \neq i$, on species i. If $L_i = 0$, then there is no inhibition, so that μ_i depends only on S_i.

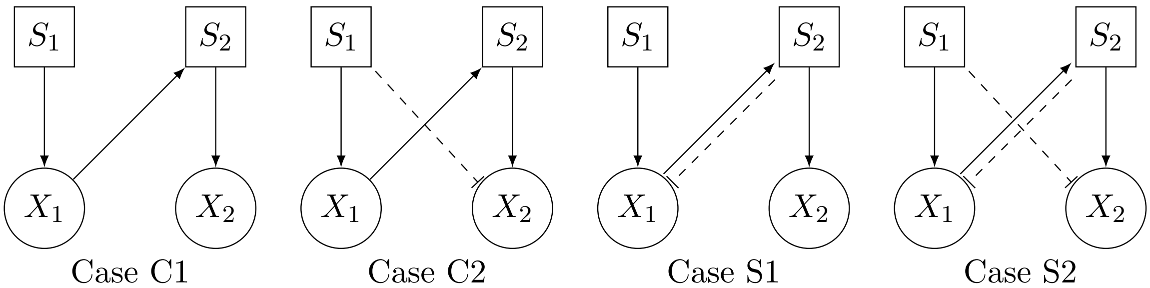

Figure 1: Commensalistic and syntrophic systems without self inhibition.

In Fig. 1, we illustrate (2.1) by using the notations and representations of microbial communities proposed by Di and Yang [17]. Species X_2 is produced by consuming chemical S_2 which itself is produced by species X_1 through consuming chemical S_1 that acts as the substrate of the overall system. The system C1, which corresponds to $L_1 = L_2 = 0$ in (2.3), is an example of pure commensalism, where the second population (the commensal population) depends for its growth on the first population (the host) and thus, benefits from its interaction, while the host population is not affected by the growth of the commensal population. The system C2, which corresponds to $L_1 = 0$ and $L_2 > 0$ in (2.3), is also an example of commensalism, since it has a cascade structure, and the first population is not affected by the growth of the second population.

On the other hand the systems S1, which corresponds to $L_1 > 0$ and $L_2 = 0$ in (2.3), and S2, which corresponds to $L_1 > 0$ and $L_2 > 0$ in (2.3), are not commensal, since the first population is affected by the growth of the second population. For instance, in S1, the first organism is inhibited by the substrate S_2 produced by the degradation of S_1 by X_1. Hence, the extent to which the substrate S_1 is degraded by the organism X_1 to produce the substrate S_2 which is necessary for the growth of X_2, depends on the efficiency of the removal of the product S_2 by the bacteria X_2. Therefore, each population needs the other one for its growth, that is, there is a syntrophic relationship between them.

Remark 1. *Case C1 corresponds to the base system depicted on Fig. 1 of [17]. Cases C2, S1 and S2 correspond, respectively, to cases 1-4, 1-1 and 2-3, shown in Figs. 2 and 3 of [17]. Notice that [17] considered also inhibitions between species, see cases 1-2 and 1-3 in Fig. 2 of [17] and five other systems obtained by combining them, see Fig. 3 of [17]. Although very important for microbial ecology, these species inhibitions will not be considered in this paper. The models C1, C2, S1 and S2 have been extensively studied in the literature, see Tables 10 and 11 in Appendix E.*

There are many ways of representing inhibition other than (2.3). For example, instead of decreasing the maximum growth rate m_i of the Monod function as in (2.3), we can increase its half-velocity constant (or substrate affinity) K_i:

$$\mu_1(S_1, S_2) = \frac{m_1 S_1}{K_1 + L_1 S_2 + S_1}, \qquad \mu_2(S_1, S_2) = \frac{m_2 S_2}{K_2 + L_2 S_1 + S_2}, \tag{2.4}$$

where L_i quantifies the strength of inhibition of S_j on species i. See also the Kreikenbohm and Bohl function KB1 in Table 14.

In this work, instead of considering particular growth functions as (2.3), (2.4) or KB1, we consider generalized growth functions characterized by their qualitative behaviors. Assume that $\mu_1, \mu_2 : \mathbb{R}_+^2 \to \mathbb{R}_+$ are of class C^1, such that $\mu_1(0, S_2) = 0$ for $S_2 \geq 0$ and $\mu_2(S_1, 0) = 0$ for $S_1 \geq 0$. Hence, no growth takes place for species $i = 1, 2$ without substrate S_i. This hypothesis is made in all the paper and will not be repeated. The solutions of (2.1), with prescribed initial conditions, exist, are unique, are bounded, and the non-negative cone is positively invariant. The positive cone is also positively invariant. We make the following assumptions

H1 For $S_1 > 0$ and $S_2 \geq 0$, we have $\frac{\partial \mu_1}{\partial S_1}(S_1, S_2) > 0$ and $\frac{\partial \mu_1}{\partial S_2}(S_1, S_2) \leq 0$.

H2 For $S_1 \geq 0$ and $S_2 > 0$, we have $\frac{\partial \mu_2}{\partial S_2}(S_1, S_2) > 0$ and $\frac{\partial \mu_2}{\partial S_1}(S_1, S_2) \leq 0$.

Hypotheses **H1** and **H2** signify that the growth for species $i = 1, 2$ increases with S_i, while it is inhibited by the other substrate S_j, $j \neq i$: the first organism is inhibited by its product S_2 and the second organism is inhibited by the food S_1 of the first organism.

Remark 2. *Since the partial derivative $\frac{\partial \mu_i}{\partial S_j}(S_1, S_2)$, for $j \neq i$, can be equal to zero, the inhibition of species i by substrate $j \neq i$ is not mandatory. Hence, the assumptions* **H1** *and* **H2** *cover the cases C1, C2, S1 and S2 of Fig. 1. For example, C1 corresponds to μ_1 depending only on S_1 and increasing for all $S_1 > 0$ and μ_2 depending only on S_2 and increasing for all $S_2 > 0$.*

To reduce the number of parameters, the model (2.1) is further converted to a simpler one where the yield factors k_i are fixed to 1. We scale system (2.1) using the following change of variables and notations :

$$s_1 = k_3 S_1/k_1,\ x_1 = k_3 X_1,\ s_2 = S_2,\ x_2 = k_2 X_2,\ s_1^{in} = k_3 S_1^{in}/k_1,\ s_2^{in} = S_2^{in}.$$

We obtain the following system of differential equations

$$\begin{aligned} \dot{s}_1 &= D\left(s_1^{in} - s_1\right) - f_1(s_1, s_2)\, x_1, \\ \dot{x}_1 &= \left(f_1(s_1, s_2) - D_1\right) x_1, \\ \dot{s}_2 &= D\left(s_2^{in} - s_2\right) + f_1(s_1, s_2)\, x_1 - f_2(s_1, s_2)\, x_2, \\ \dot{x}_2 &= \left(f_2(s_1, s_2) - D_2\right) x_2, \end{aligned} \tag{2.5}$$

where the yield factors k_i are fixed to 1 and the growth functions $f_1, f_2 : \mathbb{R}_+^2 \to \mathbb{R}_+$ are given by

$$f_1(s_1, s_2) = \mu_1\left(k_1 s_1/k_3, s_2\right) \quad \text{and} \quad f_2(s_1, s_2) = \mu_2\left(k_1 s_1/k_3, s_2\right). \tag{2.6}$$

Since μ_i, $i = 1, 2$ in (2.1) satisfy the conditions **H1** and **H2**, then the growth functions f_i, $i = 1, 2$ in (2.5) have the same qualitative properties.

3 Results

3.1 Graphical method

In this section, we explain the graphical method of [3, 50, 51].

3.1.1 The feasible set boundary (FSB)

The "feasible set" $\mathcal{F}$ is the set of point $(s_1, s_2) \in \mathbb{R}^2_+$, where the (s_1, s_2)-coordinate of any equilibrium point must be located. We have the following result.

Lemma 1. *If $E = (s_1, x_1, s_2, x_2)$ is an equilibrium point of (2.5), then $0 < s_1 \leq s_1^{in}$, $0 < s_2 \leq s_1^{in} + s_2^{in} - s_1$ and*

$$x_1 = \tfrac{D}{D_1}\left(s_1^{in} - s_1\right), \quad x_2 = \tfrac{D}{D_2}\left(s_1^{in} + s_2^{in} - s_1 - s_2\right). \tag{3.1}$$

Proof. The equilibria of the system are the solutions of the following set of equations obtained by setting the right-hand sides of equations in (2.5) equal to zero

$$0 = D\left(s_1^{in} - s_1\right) - f_1(s_1, s_2)\, x_1, \tag{3.2}$$

$$0 = (f_1(s_1, s_2) - D_1)\, x_1, \tag{3.3}$$

$$0 = D\left(s_2^{in} - s_2\right) + f_1(s_1, s_2)\, x_1 - f_2(s_1, s_2)\, x_2, \tag{3.4}$$

$$0 = (f_2(s_1, s_2) - D_2)\, x_2. \tag{3.5}$$

At an equilibrium point we necessarily have $s_1 > 0$ and $s_2 > 0$.Using (3.2)+(3.3) and (3.4)+(3.5)-(3.3), we obtain the equations

$$0 = D\left(s_1^{in} - s_1\right) - D_1 x_1, \quad 0 = D\left(s_2^{in} - s_2\right) + D_1 x_1 - D_2 x_2.$$

By solving these equations, we obtain x_1 and x_2 as functions of s_1 and s_2, as given by (3.1). Consequently, the requirement that the components x_i are non-negative imposes that the coordinates (s_1, s_2) of an equilibrium point must satisfy $s_1 \leq s_1^{in}$ and $s_1 + s_2 \leq s_1^{in} + s_2^{in}$. □

Therefore, the feasible set is given by:

$$\mathcal{F} = \left\{(s_1, s_2) \in \mathbb{R}^2_+ : 0 < s_1 \leq s_1^{in}, \quad 0 < s_2 \leq s_1^{in} + s_2^{in} - s_1\right\}.$$

The boundary of $\mathcal{F}$ consists of two portions of the coordinate axes, together with two curves, namely the *feasible set boundary* FSB_i for population i, defined as follows

$$\begin{array}{l} \mathrm{FSB}_1 = \left\{(s_1, s_2) \in \mathbb{R}^2_+ : s_1 = s_1^{in},\ 0 < s_2 \leq s_2^{in}\right\}, \\ \mathrm{FSB}_2 = \left\{(s_1, s_2) \in \mathbb{R}^2_+ :\ 0 < s_1 \leq s_1^{in},\ s_1 + s_2 = s_1^{in} + s_2^{in}\right\}. \end{array} \tag{3.6}$$

These line segments are plotted in green and red respectively in Figs. 2 and 3.

Remark 3. *The formulas* (3.1) *show that the x_1 and x_2 components of an equilibrium point are uniquely determined by its s_1 and s_2 components. This is why we can, without risk of confusion, denote by the same notation an equilibrium point and its projection* (s_1, s_2) *on the feasible set, as we do in Figs. 2 and 3. We will use this abuse of notation in all the figures.*

3.1.2 The zero net growth isocline (ZNGI) and the equilibria

Then we construct the ZNGI for each population and plot them in (s_1, s_2)-plane using the same color used for population i as used for its FSB_i. The ZNGI for population i, denoted ZNGI_i, is the curve of substrate concentrations along which the decline in biomass density is balanced by its growth. Therefore

$$\mathrm{ZNGI}_i = \left\{(s_1, s_2) \in \mathbb{R}^2_+ : f_i(s_1, s_2) = D_i\right\}, \qquad i = 1, 2. \tag{3.7}$$

The following step is to identify equilibria: each intersection of a green curve and a red curve in the feasible set corresponds to an equilibrium point, i.e. is the projection on the feasible set of an equilibrium point, as depicted in Figs. 2 and 3. More precisely, we have the following result.

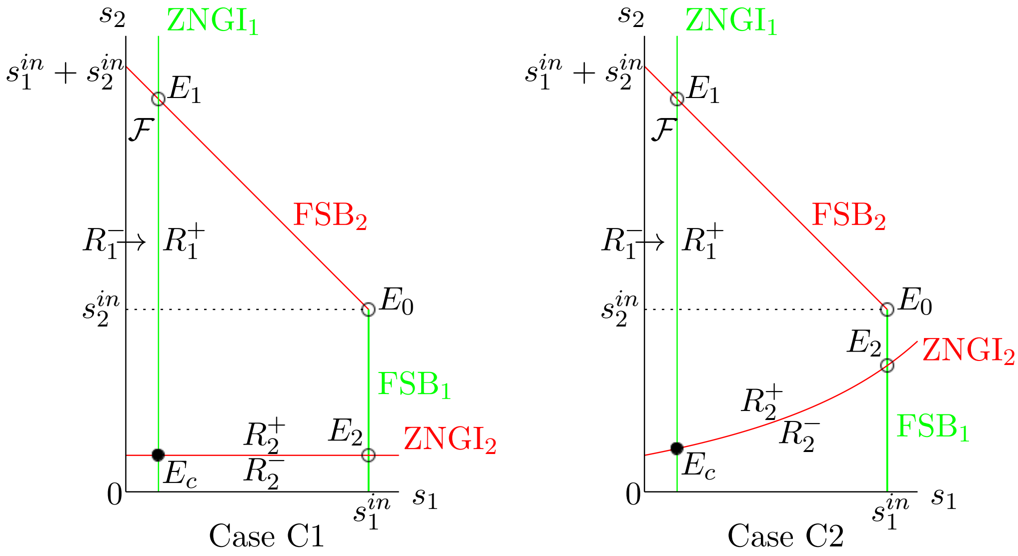

Figure 2: The feasible set $\mathcal{F}$, the ZNGIs and the regions R_1^-, R_1^+, R_2^+ and R_2^-, for the commensalistic cases C1 and C2.

Lemma 2.
- *The intersection point* $\left(s_1^{in}, s_2^{in}\right) = \text{FSB}_1 \cap \text{FSB}_2$ *corresponds to the washout equilibrium* $E_0 = \left(s_1^{in}, 0, s_2^{in}, 0\right)$ *where both species are extinct.*
- *Any point* $(\bar{s}_1, \bar{s}_2) \in \text{ZNGI}_1 \cap \text{FSB}_2$ *corresponds to a boundary equilibrium* $E_1 = (\bar{s}_1, \bar{x}_1, \bar{s}_2, 0)$*, where species 2 is absent and species 1 is present.*
- *Any point* $(\tilde{s}_1, \tilde{s}_2) \in \text{FSB}_1 \cap \text{ZNGI}_2$ *corresponds to a boundary equilibrium* $E_2 = (\tilde{s}_1, 0, \tilde{s}_2, \tilde{x}_2)$*, where species 1 is absent and species 2 is present.*
- *Any point* $\left(s_1^*, s_2^*\right) \in \text{ZNGI}_1 \cap \text{ZNGI}_2$ *lying in the interior* $\mathcal{F}^o$ *of the feasible set* $\mathcal{F}$ *corresponds to a coexistence equilibrium* $E_c = \left(s_1^*, x_1^*, s_2^*, x_2^*\right)$*, where both species are present.*

Proof. Recall that an equilibrium point $E = (s_1, x_1, s_2, x_2)$ is a solution of equations (3.2)-(3.5). Four cases must be distinguished:

1) Assume that $x_1 = x_2 = 0$, which corresponds to the washout equilibrium point E_0. Then, from (3.2) and $x_1 = 0$ it is deduced that $s_1 = s_1^{in}$ and from (3.4) and $x_2 = 0$, it is deduced that $s_2 = s_2^{in}$. Hence $(s_1, s_2) = \left(s_1^{in}, s_2^{in}\right) = \text{FSB}_1 \cap \text{FSB}_2$.

2) Assume that $x_1 > 0$ and $x_2 = 0$, which corresponds to a boundary equilibrium point E_1. Then, from (3.3) and $x_1 > 0$ it is deduced that $f_1(s_1, s_2) = D_1$. Therefore $(s_1, s_2) \in \text{ZNGI}_1$. Using now (3.2)+(3.4), we obtain

$$0 = D\left(s_1^{in} + s_2^{in} - s_1 - s_2\right) - f_2(s_1, s_2)x_2. \tag{3.8}$$

From $x_2 = 0$ and (3.8) we deduce that $s_1 + s_2 = s_1^{in} + s_2^{in}$. Using now $x_1 > 0$, from (3.1) we deduce that $s_1 < s_1^{in}$. Therefore $(s_1, s_2) \in \text{FSB}_2$. Hence, $(s_1, s_2) \in \text{ZNGI}_1 \cap \text{FSB}_2$.

3) Assume that $x_1 = 0$ and $x_2 > 0$, which corresponds to a boundary equilibrium point E_2. Then, from $x_1 = 0$ and (3.2) we deduce that $s_1 = s_1^{in}$. Using now $x_2 > 0$, from (3.1) we deduce that $s_2 < s_2^{in}$. Therefore $(s_1, s_2) \in \text{FSB}_1$. From $x_2 > 0$ and (3.5) we have $f_2(s_1, s_2) = D_2$. Therefore $(s_1, s_2) \in \text{ZNGI}_2$. Hence, $(s_1, s_2) \in \text{FSB}_1 \cap \text{ZNGI}_2$.

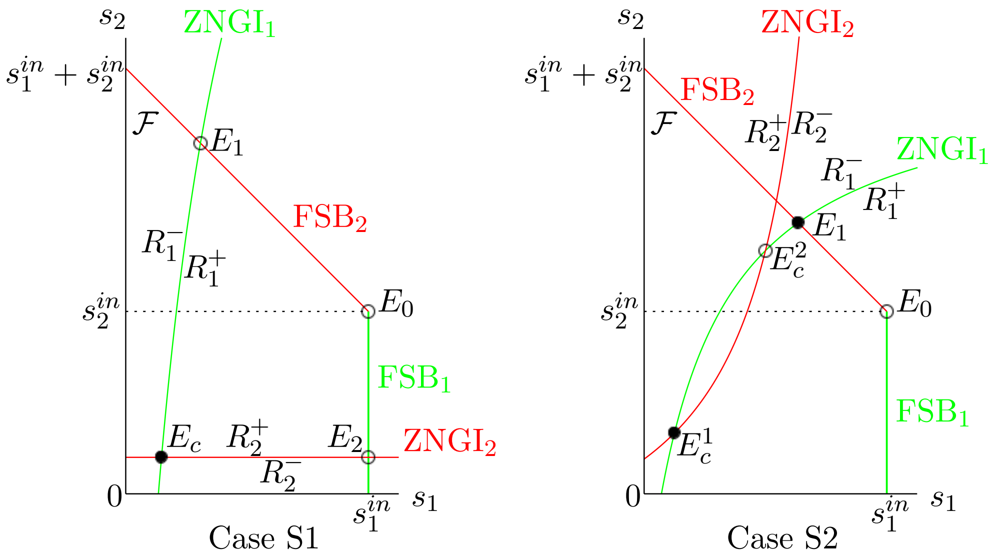

Figure 3: The feasible set $\mathcal{F}$, the ZNGIs and the regions R_1^-, R_1^+, R_2^+ and R_2^-, for the syntrophic cases S1 and S2.

4) If $x_1 > 0$ and $x_2 > 0$, which corresponds to a coexistence equilibrium point E_c, then, from $x_1 > 0$ and (3.3) we have $f_1(s_1, s_2) = D_1$ and from $x_2 > 0$ and (3.5), we have $f_2(s_1, s_2) = D_2$. Therefore, $(s_1, s_2) \in \text{ZNGI}_1 \cap \text{ZNGI}_2$. The equilibrium point E_c exists if and only if x_1 and x_2 are positive, i.e. $(s_1, s_2) \in \mathcal{F}^o$. □

3.1.3 Existence and stability of equilibria

The last step is to determine the conditions of existence and stability of equilibria, which result from their location with respect to the ZNGIs. A stable equilibrium is plotted with a solid circle and an unstable one with a circle, as depicted in Figs. 2 and 3. This convention will be used in all figures.

The washout equilibrium E_0 is unique and always exists. The number and nature of the boundary and positive equilibria depend on the relative positions of the ZNGIs. The stability of E_0, as well as the existence, uniqueness and stability of the other equilibrium points, require the use of assumptions **H1** and **H2** on the growth functions μ_1 and μ_2. Since the growth functions f_1 and f_2 are given by (2.6), they satisfy the following conditions, where we use the notations $f_{ij} = \partial f_i / \partial s_j$, $i, j = 1, 2$, for the partial derivatives.

$$\text{For } s_1 > 0, s_2 \geq 0, \quad f_{11}(s_1, s_2) > 0 \text{ and } f_{12}(s_1, s_2) \leq 0. \tag{3.9}$$

$$\text{For } s_1 \geq 0, s_2 > 0, \quad f_{21}(s_1, s_2) \leq 0 \text{ and } f_{22}(s_1, s_2) > 0. \tag{3.10}$$

In order to describe the ZNGIs, it is convenient to use the concept of break-even concentration.

Definition 1. *Let $m_1(s_2) = f_1(+\infty, s_2) = \sup_{s_1>0} f_1(s_1, s_2)$. For $s_2 \geq 0$ and $D \in [0, m_1(s_2))$, the break-even concentration is the unique solution $s_1 = \lambda_1(s_2, D)$ of equation $f_1(s_1, s_2) = D$.*
Let $m_2(s_1) = f_2(s_1, +\infty) = \sup_{s_2>0} f_2(s_1, s_2)$. For $s_1 \geq 0$ and $D \in [0, m_2(s_1))$, the break-even concentration is the unique solution $s_2 = \lambda_2(s_1, D)$ of equation $f_2(s_1, s_2) = D$.

Notice that the existence and uniqueness of $s_1 = \lambda_1(s_2, D)$ follows from (3.9), since $\partial f_1/\partial s_1 > 0$ for all $s_1 > 0$. Using the implicit function theorem one sees that $\partial\lambda_1/\partial s_2 = -f_{12}/f_{11} \geq 0$. Therefore $\lambda_1(s_2, D)$ is increasing in s_2. Similarly, $s_2 = \lambda_2(s_1, D)$ is well defined and satisfies $\partial\lambda_2/\partial s_1 = -f_{21}/f_{22} \geq 0$. Therefore, it is increasing in s_1.

Using the break-even concentrations, the ZNGIs (3.7) are given by:

$$\mathrm{ZNGI}_1 = \left\{(s_1, s_2) \in \mathbb{R}^2_+ : s_1 = \lambda_1(s_2, D_1)\right\}, \tag{3.11}$$

$$\mathrm{ZNGI}_2 = \left\{(s_1, s_2) \in \mathbb{R}^2_+ : s_2 = \lambda_2(s_1, D_2)\right\}. \tag{3.12}$$

Since ZNGI_1 is the graph of the increasing function $s_2 \mapsto s_1 = \lambda_1(s_2, D_1)$, it divides the positive cone $\mathbb{R}^2_+$ into two connected regions

$$R_1^- = \left\{(s_1, s_2) \in \mathbb{R}^2_+ : f_1(s_1, s_2) < D_1\right\}, \quad R_1^+ = \left\{(s_1, s_2) \in \mathbb{R}^2_+ : f_1(s_1, s_2) > D_1\right\}.$$

The region R_1^- contains the origin, and the region R_1^+ is possibly empty. Similarly, since ZNGI_2 is the graph of the increasing function $s_1 \mapsto s_2 = \lambda_2(s_1, D_2)$, it divides the positive cone $\mathbb{R}^2_+$ into two connected regions

$$R_2^- = \left\{(s_1, s_2) \in \mathbb{R}^2_+ : f_2(s_1, s_2) < D_2\right\}, \quad R_2^+ = \left\{(s_1, s_2) \in \mathbb{R}^2_+ : f_2(s_1, s_2) > D_2\right\}.$$

The region R_2^- contains the origin, and the region R_2^+ is possibly empty.

We say that an equilibrium is stable if it is locally exponentially stable, i.e. the Jacobian matrix has eigenvalues with strictly negative real parts. We can give now the main result

Proposition 3. *Assume that* (3.9) *and* (3.10) *are satisfied. The conditions of existence and stability of the equilibria of (2.5) are given in Table 1.*

Proof. The proof is given in Appendix D.1. □

Table 1: Conditions of existence and stability of the equilibria of (2.5). Here $(\mathrm{ZNGI}_1, \mathrm{ZNGI}_2)$ is the signed angle between ZNGI_1 and ZNGI_2 at E_c.

	Existence condition	Stability condition (local)
$E_0 = \mathrm{FSB}_1 \cap \mathrm{FSB}_2$	Always exists	$E_0 \in R_1^- \cap R_2^-$
$E_1 = \mathrm{ZNGI}_1 \cap \mathrm{FSB}_2$	$E_0 \in R_1^+$	$E_1 \in R_2^-$
$E_2 = \mathrm{FSB}_1 \cap \mathrm{ZNGI}_2$	$E_0 \in R_2^+$	$E_2 \in R_1^-$
$E_c \in \mathrm{ZNGI}_1 \cap \mathrm{ZNGI}_2$	$E_c \in \mathcal{F}^o$	$(\mathrm{ZNGI}_1, \mathrm{ZNGI}_2) < 0$

In Table 1, $(\mathrm{ZNGI}_1, \mathrm{ZNGI}_2)$ is the signed angle between ZNGI_1 and ZNGI_2 at their intersection point E_c. As it is usual, we define the signed angle between two intersecting curves to be the signed angle between the tangents at the point of intersection.

We have thus obtained a complete description of the existence and stability conditions of the equilibria of (2.5), simply by considering the location of their projections on the feasible set $\mathcal{F}$. Existence of the equilibria is determined from the intersections of the ZNGIs and FSBs plotted with different colors. Stability of the equilibria is determined from the location of the projections of the equilibria E_0, E_1, E_2 and E_c, in the regions R_1^-, R_1^+, R_2^+ and R_2^- of the feasible set $\mathcal{F}$. Let us illustrate these results in the cases shown in Figs. 2 and 3.

- On these figures E_0 is unstable since $E_0 \notin R_1^- \cap R_2^-$ and E_1 exists since $E_0 \in R_1^+$. On Fig. 2 and Fig. 3 (Case S1), E_1 is unstable since $E_1 \notin R_2^-$. On Fig. 3 (Case S2), E_1 is stable since $E_1 \in R_2^-$.
- On Fig. 2 and Fig. 3 (Case S1), E_2 exists since $E_0 \in R_2^+$ and is unstable since $E_2 \notin R_1^-$. On Fig. 3 (Case S2), E_2 does not exist since $E_0 \notin R_2^+$.
- On Fig. 2 and Fig. 3 (Case S1), E_c is unique and stable since, at E_c, $(\mathrm{ZNGI}_1, \mathrm{ZNGI}_2) < 0$.
- On Fig. 3 (Case S2), E_c^1 is stable since, at E_c^1, $(\mathrm{ZNGI}_1, \mathrm{ZNGI}_2) < 0$, and E_c^2 is unstable since, at E_c^2, $(\mathrm{ZNGI}_1, \mathrm{ZNGI}_2) > 0$.

3.2 Operating diagram

In this section, we describe the operating diagram of (2.5). Since the system (2.5) has three operating parameters, and it is not easy to visualize regions in the three-dimensional operating parameter space, we fix the dilution rate D and we show the operating diagram in the operating plane $\left(s_1^{in}, s_2^{in}\right)$. The effects of D can be shown in a series of operating diagrams, see Fig. 9. In Section A, we fix the operating parameter s_2^{in} and we show the operating diagram in the operating plane $\left(s_1^{in}, D\right)$. The effects of s_2^{in} can be shown in a series of operating diagrams, see Figs. 15, 17 and 18.

We fix the growth functions f_i and the parameters α_i and a_i, $i = 1, 2$. We begin with the more simple cases C1, C2 and S1. We see in Figs. 2 and 3 (Case S1) that the ZNGIs have a unique intersection point $\left(s_1^*(D), s_2^*(D)\right) := \mathrm{ZNGI}_1 \cap \mathrm{ZNGI}_2$.

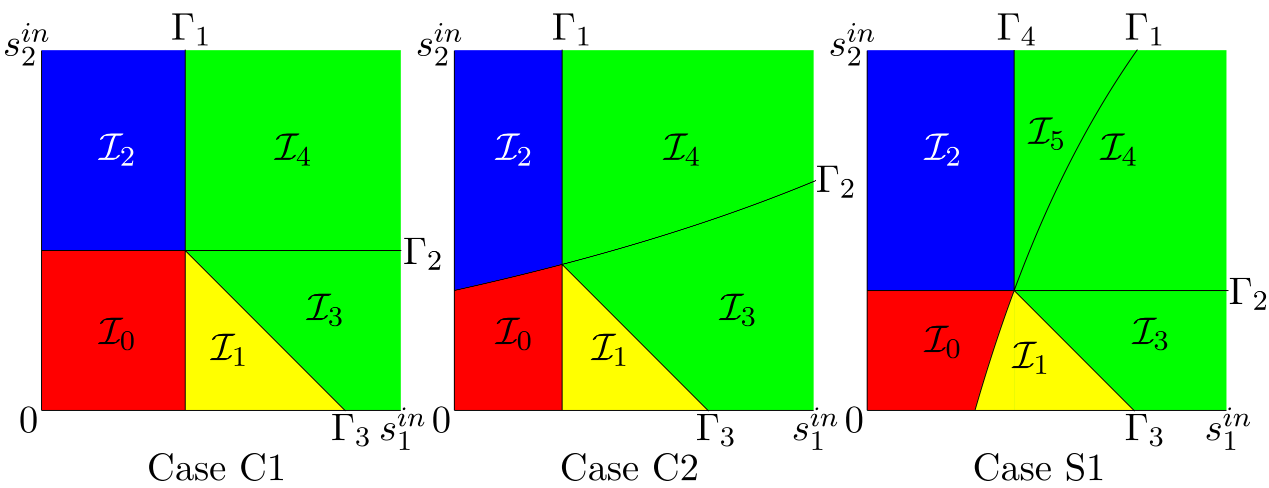

Figure 4: The operating diagram in the operating plane $\left(s_1^{in}, s_2^{in}\right)$ and $0 < D < \min(\delta_1, \delta_2)$, where δ_i are defined by (3.16). The asymptotic behavior in the various regions of the operating diagram is shown in Table 2 for cases C1 and C2, and in Table 3 for case S1. The case $D \geq \min(\delta_1, \delta_2)$ is shown in Fig. 6.

Table 2: Existence and stability of equilibria of (2.5) in the regions of the operating diagram depicted in Fig. 4 (Cases C1 and C2). The letter U means that the equilibrium is unstable, GAS means that it is globally asymptotically stable. No letter means that it does not exist.

	E_0	E_1	E_2	E_c	Color
$\mathcal{I}_0$	GAS				Red
$\mathcal{I}_1$	U	GAS			Yellow
$\mathcal{I}_2$	U		GAS		Blue
$\mathcal{I}_3$	U	U		GAS	Green
$\mathcal{I}_4$	U	U	U	GAS	Green

Table 3: Existence and stability of equilibria of (2.5) in the regions of the operating diagram depicted in Fig. 4 (Case S1). The letter S means that the equilibrium is locally exponentially stable. If $D_1 = D_2 = D$, the letter S should be replaced by GAS.

	E_0	E_1	E_2	E_c	Color
$\mathcal{I}_0$	S				Red
$\mathcal{I}_1$	U	S			Yellow
$\mathcal{I}_2$	U		S		Blue
$\mathcal{I}_3$	U	U		S	Green
$\mathcal{I}_4$	U	U	U	S	Green
$\mathcal{I}_5$	U		U	S	Green

3.2.1 Commensalism (Cases C1 and C2)

We consider the curves

$$\Gamma_i \quad = \quad \left\{ \left(s_1^{in}, s_2^{in}\right) \in \mathbb{R}_+^2 : f_i\left(s_1^{in}, s_2^{in}\right) = D_i \right\}, \quad i = 1, 2. \tag{3.13}$$

Even though Γ_i are defined by the same equations as the ZNGIs, see (3.7), it should be noted that Γ_i are curves in the plane of operating parameters $\left(s_1^{in}, s_2^{in}\right)$, while ZNGI$_i$ are curves in the phase plane (s_1, s_2). The curves Γ_1 and Γ_2, defined by 3.13, together with the curve Γ_3 given by

$$\Gamma_3 \quad = \quad \left\{ \left(s_1^{in}, s_2^{in}\right) \in \mathbb{R}_+^2 : s_1^{in} + s_2^{in} = s_1^*(D) + s_2^*(D) \text{ and } s_1^{in} > s_1^*(D) \right\}, \tag{3.14}$$

divide the set of operating parameters $\left(s_1^{in}, s_2^{in}\right)$ in five regions denoted $\mathcal{I}_k$, $k = 0, \ldots, 4$, see Fig. 4. For the C1 case we have:

- Γ_1 is the vertical line of equation $s_1^{in} = \lambda_1(D_1)$,
- Γ_2 is the horizontal line of equation $s_2^{in} = \lambda_2(D_2)$,
- Γ_3 is the oblique line of equation $s_1^{in} + s_2^{in} = \lambda_1(D_1) + \lambda_2(D_2)$.

The novelty when we consider the C2 case is that Γ_2 becomes the curve of equation $s_2^{in} = \lambda_2\left(s_1^{in}, D_2\right)$. We have the following result:

Proposition 4. *The condition of existence and stability of the equilibria of the C1 and C2 models in the regions $\mathcal{I}_k$, $k = 0, \ldots, 4$ of Fig. 4 (Case C1 or C2) are given in Table 2.*

Proof. The proof consists simply in looking at the location of the equilibria in the feasible set and applying Proposition 3. We give the details for the case C1. Assume that $\left(s_1^{in}, s_2^{in}\right) \in \mathcal{I}_4$. We see in Fig. 5 that E_0 is unstable since $E_0 \notin R_1^- \cap R_2^-$, E_1 exists since $E_0 \in R_1^+$ and is unstable, since $E_1 \notin R_2^-$, E_2 exits since $E_0 \in R_2^+$ and is unstable since $E_2 \notin R_1^-$, and E_c exists, is unique and stable since, at E_c, we have $(\text{ZNGI}_1, \text{ZNGI}_2) < 0$. The proof for global asymptotic stability is given in Section B.1. This proves the results depicted in the last row of Table 2. The proofs for the other regions are illustrated in Fig. 5. The details of the proof for the C2 case are given in Appendix D.2. □

Although the regions $\mathcal{I}_3$ and $\mathcal{I}_4$ are different in terms of the existence of equilibria, they are coloured green because they correspond to the stability of the coexistence equilibrium E_c.

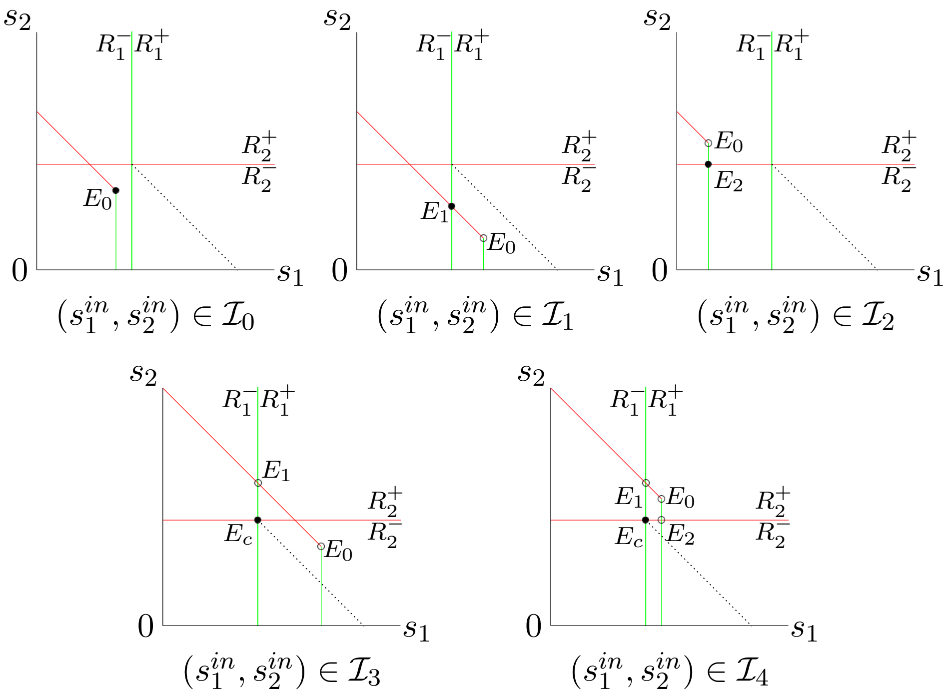

Figure 5: Proof of Proposition 4 in the case C1: feasible sets and ZNGIs, showing equilibria and their stability, for the four regions of the operating diagram, shown in Fig. 4 (Case C1).

3.2.2 Pure syntrophy (Case S1)

In addition to the curves Γ_1 and Γ_2, defined by (3.13), and the curve and Γ_3, defined by (3.14), consider the line segment defined by:

$$\Gamma_4 = \left\{ \left(s_1^{in}, s_2^{in}\right) \in \mathbb{R}_+^2 : s_1^{in} = s_1^*(D) \text{ and } s_2^{in} > s_2^*(D) \right\}. \tag{3.15}$$

The novelty when we consider model S1 is that the curve Γ_1 becomes the curve of equation $s_1^{in} = \lambda_1\left(s_2^{in}, D_1\right)$, and is therefore distinct from Γ_4, which is the vertical line of equation $s_1^{in} = s_1^*(D)$. Therefore, in the S1 case, the curves Γ_i, $i = 1, \ldots, 4$, defined by (3.13), (3.14) and (3.15) divide the set of operating parameters $\left(s_1^{in}, s_2^{in}\right)$ in six regions denoted $\mathcal{I}_k$, $k = 0, \ldots, 5$, see Fig. 4 (Case S1). We have the following result:

Proposition 5. *The conditions of existence and stability of the equilibria of the S1 model in the regions $\mathcal{I}_k$, $k = 0, \ldots, 5$ of Fig. 4 (Case S1) are given in Table 3.*

Proof. The proof is given in Appendix D.3. □

Although the regions $\mathcal{I}_3$, $\mathcal{I}_4$ and $\mathcal{I}_5$ are different in terms of the existence of equilibria, they are coloured green because all three correspond to the stability of the coexistence equilibrium E_c.

The number of regions in the operating plane $\left(s_1^{in}, s_2^{in}\right)$ depends on D. More precisely, let us define

$$\begin{array}{lll} \text{For C1:} & \delta_1 = (m_1 - a_1)/\alpha_1, & \delta_2 = (m_2 - a_2)/\alpha_2, \\ \text{For C2:} & \delta_1 = (m_1 - a_1)/\alpha_1, & \delta_2 = (m_2(0) - a_2)/\alpha_2, \\ \text{For S1:} & \delta_1 = (m_1(0) - a_1)/\alpha_1, & \delta_2 = (m_2 - a_2)/\alpha_2. \end{array} \tag{3.16}$$

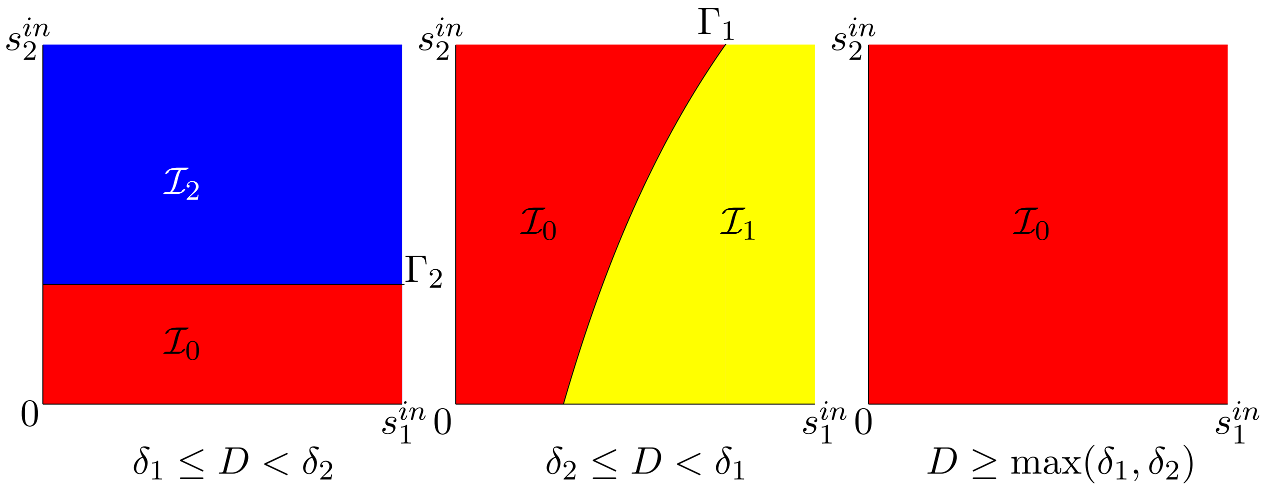

Figure 6: The operating diagram of model S1 in the operating plane $\left(s_1^{in}, s_2^{in}\right)$ and $D \geq \min(\delta_1, \delta_2)$, where δ_i are defined by (3.16).

If $0 < D < \min(\delta_1, \delta_2)$, then all regions $\mathcal{I}_k$, $k = 0, \ldots, 4$, appear as shown in Fig. 4. If $\delta_1 < \delta_2$ and $\delta_1 \leq D < \delta_2$, only $\mathcal{I}_0$ and $\mathcal{I}_2$ appear. If $\delta_2 < \delta_1$ and $\delta_2 \leq D < \delta_1$, only $\mathcal{I}_0$ and $\mathcal{I}_1$ appear. Finally, if $D \geq \max(\delta_1, \delta_2)$ then the region $\mathcal{I}_0$ invades the whole plane, see Fig. 6.

3.2.3 The S2 case

To simplify the analysis, we assume that the ZNGIs intersect in two points, as in Fig. 3 (Case S2). Cases with more than two intersections can be studied in the same way. More precisely, we make the following assumption.

H3 There exists $\delta_0 > 0$ such that, for all $D \in (0, \delta_0)$, the ZNGIs have two distinct intersection points $\left(s_1^{*1}(D), s_2^{*1}(D)\right)$ and $\left(s_1^{*2}(D), s_2^{*2}(D)\right)$; for $D = \delta_0$ the ZNGIs are tangent, and for $D > \delta_0$ there is no intersection.

In this case, the line segments Γ_3 and Γ_4 defined in (3.14) and (3.15), respectively, must be defined for each intersection point of the ZNGIs. More precisely, we consider the curves

$$\begin{array}{rcl} \Gamma_3^j & = & \left\{\left(s_1^{*2}(D), s_2^{*2}(D)\right) \in \mathbb{R}_+^2 : s_1^{in} + s_2^{in} = s_1^{*j}(D) + s_2^{*j}(D) \text{ and } s_1^{in} \geq s_1^{*j}(D)\right\} \\ \Gamma_4^j & = & \left\{\left(s_1^{*2}(D), s_2^{*2}(D)\right) \in \mathbb{R}_+^2 : s_1^{in} = s_1^{*j}(D) \text{ and } s_2^{in} \geq s_2^{*j}(D)\right\} \end{array}, \quad j = 1, 2. \tag{3.17}$$

The curves Γ_1 and Γ_2 defined by (3.13) and Γ_3^j, Γ_4^j, $j = 1, 2$, defined by (3.17) divide the set of operating parameters $\left(s_1^{*2}(D), s_2^{*2}(D)\right)$ in nine regions denoted $\mathcal{I}_k$, $k = 0, \ldots, 8$, see Fig. 7. According to the value of D, some of the regions can be empty, as shown in the typical example studied in Fig. 9. These regions are corresponding to different system behaviors, as stated in the following result.

Proposition 6. *The conditions of existence and stability of the equilibria of (2.5) in the regions $\mathcal{I}_k$, $k = 0, \ldots, 8$, shown in Fig. 7 are given in the table shown in this figure.*

Proof. The proof consists simply in looking at the location of the equilibria in the feasible set and apply Proposition 3. Assume that $\left(s_1^{*2}(D), s_2^{*2}(D)\right) \in \mathcal{I}_8$. We see in Fig. 8 that E_0 is unstable since $E_0 \notin R_1^- \cap R_2^-$, E_1 does not exist since $E_0 \notin R_1^+$, E_2 exists since $E_0 \in R_2^+$ and is stable since $E_2 \in R_1^-$, E_c^1 is stable since, at E_c^1,

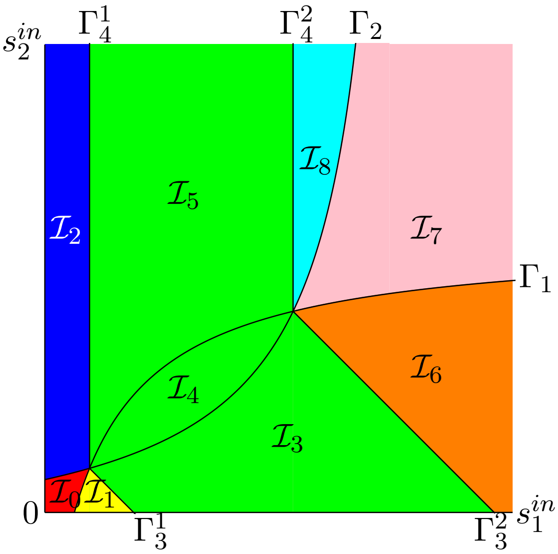

Region	E_0	E_1	E_2	E_c^1	E_c^2	Color
$\mathcal{I}_0$	S					Red
$\mathcal{I}_1$	U	S				Yellow
$\mathcal{I}_2$	U		S			Blue
$\mathcal{I}_3$	U	U		S		Green
$\mathcal{I}_4$	U	U	U	S		Green
$\mathcal{I}_5$	U		U	S		Green
$\mathcal{I}_6$	U	S		S	U	Coral
$\mathcal{I}_7$	S			S	U	Pink
$\mathcal{I}_8$	U		S	S	U	Cyan

Figure 7: The operating diagram of (2.5), in the $\left(s_1^{in}, s_2^{in}\right)$ operating plane and $D \in (0, \delta_0)$. The case $D \geq \delta_0$ is shown in Fig. 9.

we have $(\mathrm{ZNGI}_1, \mathrm{ZNGI}_2) < 0$, and E_c^2 is unstable since, at E_c^2, we have $(\mathrm{ZNGI}_1, \mathrm{ZNGI}_2) > 0$. This proves the results depicted in the last row of the table in Fig. 7. Similarly, if $\left(s_1^{*2}(D), s_2^{*2}(D)\right) \in \mathcal{I}_7$, we see in Fig. 8 that E_0 is stable since $E_0 \in R_1^- \cap R_2^-$, E_1 does not exist since $E_0 \notin R_1^+$, E_2 does not exist since $E_0 \notin R_2^+$, E_c^1 is stable since, at E_c^1, we have $(\mathrm{ZNGI}_1, \mathrm{ZNGI}_2) < 0$, and E_c^2 is unstable since, at E_c^2, we have $(\mathrm{ZNGI}_1, \mathrm{ZNGI}_2) > 0$. This proves the results described in the penultimate row of the table in Fig. 7. The proofs for the other regions are shown in Fig. 8. □

Although the regions $\mathcal{I}_3$, $\mathcal{I}_4$ and $\mathcal{I}_5$ are different in terms of the existence of equilibria, they are coloured green because all three correspond to the stability of the coexistence equilibrium E_c^1.

Table 4: The parameter values for the growth functions (2.3) used in Figs. 9.

Parameters values									
m_1	K_1	L_1	m_2	K_2	L_2	α_1	a_1	α_2	a_2
4	1	0.3	3	1	0.2	0.8	0.1	0.9	0.2

We now illustrate how the operating diagram behaves when D is varied. To do this, we consider the growth functions defined in Table 4. The operating diagrams corresponding to various values of D are shown in Fig. 9. This figure shows that as D is increased, the green regions $\mathcal{I}_3$, $\mathcal{I}_4$ and $\mathcal{I}_5$, of stability of E_c^1, shrink until they disappear completely at $D = \delta_0$. At this value of D, a saddle-node bifurcation occurs, in which E_c^1 and E_c^2 collide and annihilate each other. For $D > \delta_0$, the red region $\mathcal{I}_0$, corresponding to the stability of E_0, increases in size, until it invades the entire operating parameter plane.

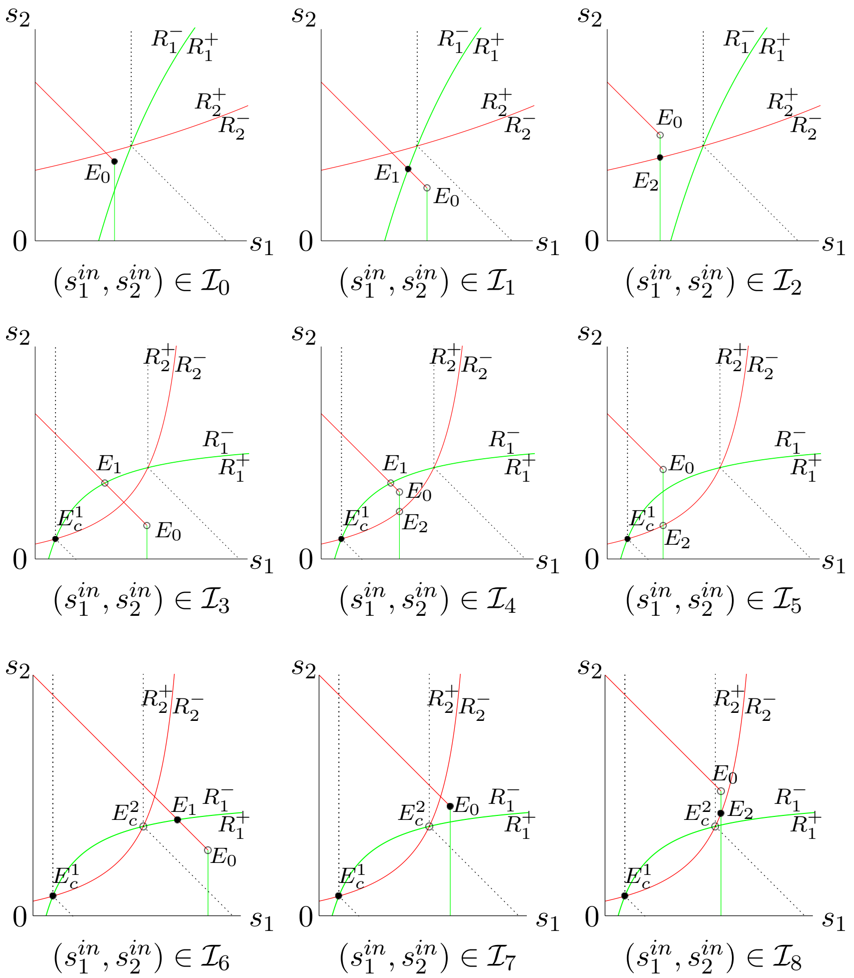

Figure 8: Proof of Proposition 6: feasible sets and ZNGIs, showing equilibria and their stability, for the nine regions of the operating diagram, shown in Fig.7.

4 Self-inhibition

4.1 Classification of models with self inhibition

In Fig. 1 we considered only the case without self inhibition of a species i by its limiting substrate S_i, as shown by the examples (2.3) and (2.4), or the general assumptions **H1** and **H2**. In this section our aim is to show that our graphical method applies without added difficulty to the case where self-inhibition is possible. For example, to represent self-inhibition, we can replace the Monod functions in (2.3) with Haldane functions and obtain:

$$\mu_1(S_1,S_2) = \frac{m_1 S_1}{K_1 + S_1 + S_1^2/K_{I1}} \frac{1}{1 + L_1 S_2}, \qquad \mu_2(S_1,S_2) = \frac{m_2 S_2}{K_2 + S_2 + S_2^2/K_{I2}} \frac{1}{1 + L_2 S_1},$$

or in (2.4) and obtain:

$$\mu_1(S_1,S_2) = \frac{m_1 S_1}{K_1 + L_1 S_2 + S_1 + S_1^2/K_{I1}}, \qquad \mu_2(S_1,S_2) = \frac{m_2 S_2}{K_2 + L_2 S_1 + S_2 + S_2^2/K_{I2}}.$$

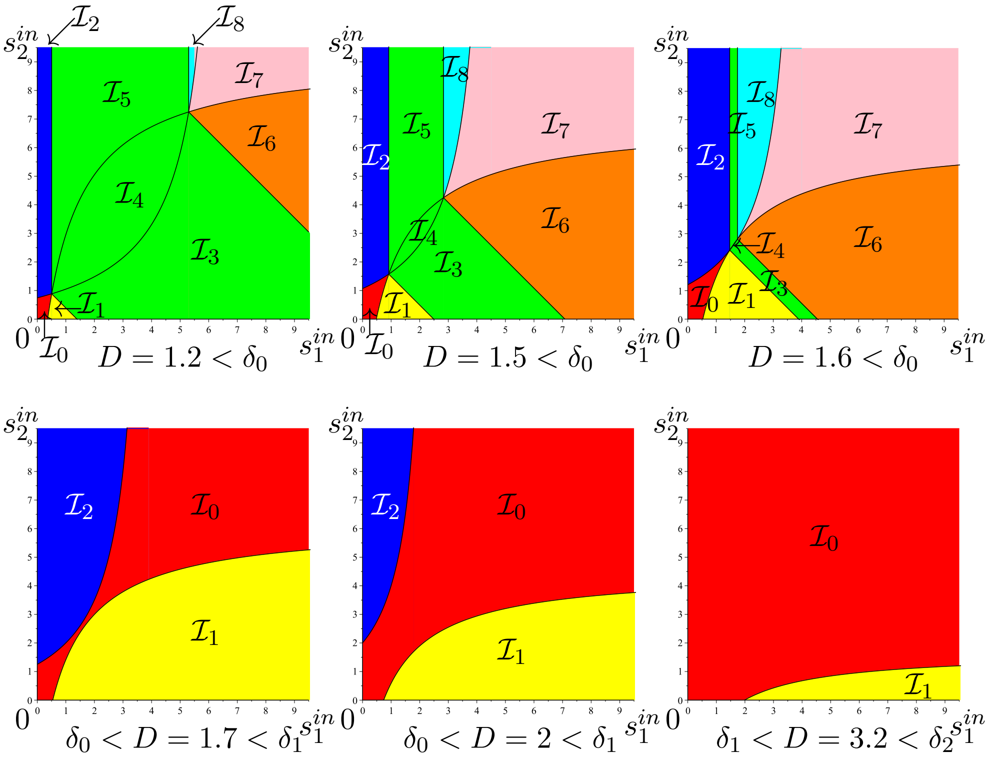

Figure 9: The operating diagram of (2.5) for the parameter values given in Table 4. Here $\delta_0 \approx 1.602$, $\delta_1 \approx 3.111$ and $\delta_2 = 4.875$. When $D > \delta_2$, region $\mathcal{I}_0$ invades the whole plane. The table showing the equilibria and their stability is the same as in Fig. 7.

See also the Kreikenbohm and Bohl function KB2 in Table 14.

In Fig. 10 we illustrate the commensalistic systems with one self inhibition, the syntrophic systems with one self inhibition, and the systems with two self inhibitions. Some of the twelve systems shown in Fig. 10 where considered in the literature, see Tables 12 and 13 in Appendix E.

We won't try to propose a general definition of inhibition, as such a definition would probably not cover all the cases of interest for applications. We will not make a full description of every case in Fig. 10 as we have done when there is no self-inhibition. Our aim is above all to show that our qualitative graphical method is applicable in each of these cases, and we will illustrate this in cases $C1_2$ and $S1_2$ which have been particularly studied in the literature, see Tables 12 and 13.

4.2 Commensalism with inhibition of the second species by its limiting substrate

We consider case $C1_2$ in Fig. 10. The model takes the form

$$
\begin{aligned}
\dot{s}_1 &= D\left(s_1^{in} - s_1\right) - f_1(s_1)\,x_1,\\
\dot{x}_1 &= \left(f_1(s_1) - D_1\right)x_1,\\
\dot{s}_2 &= D\left(s_2^{in} - s_2\right) + f_1(s_1)\,x_1 - f_2(s_2)\,x_2,\\
\dot{x}_2 &= \left(f_2(s_2) - D_2\right)x_2.
\end{aligned}
\tag{4.1}
$$

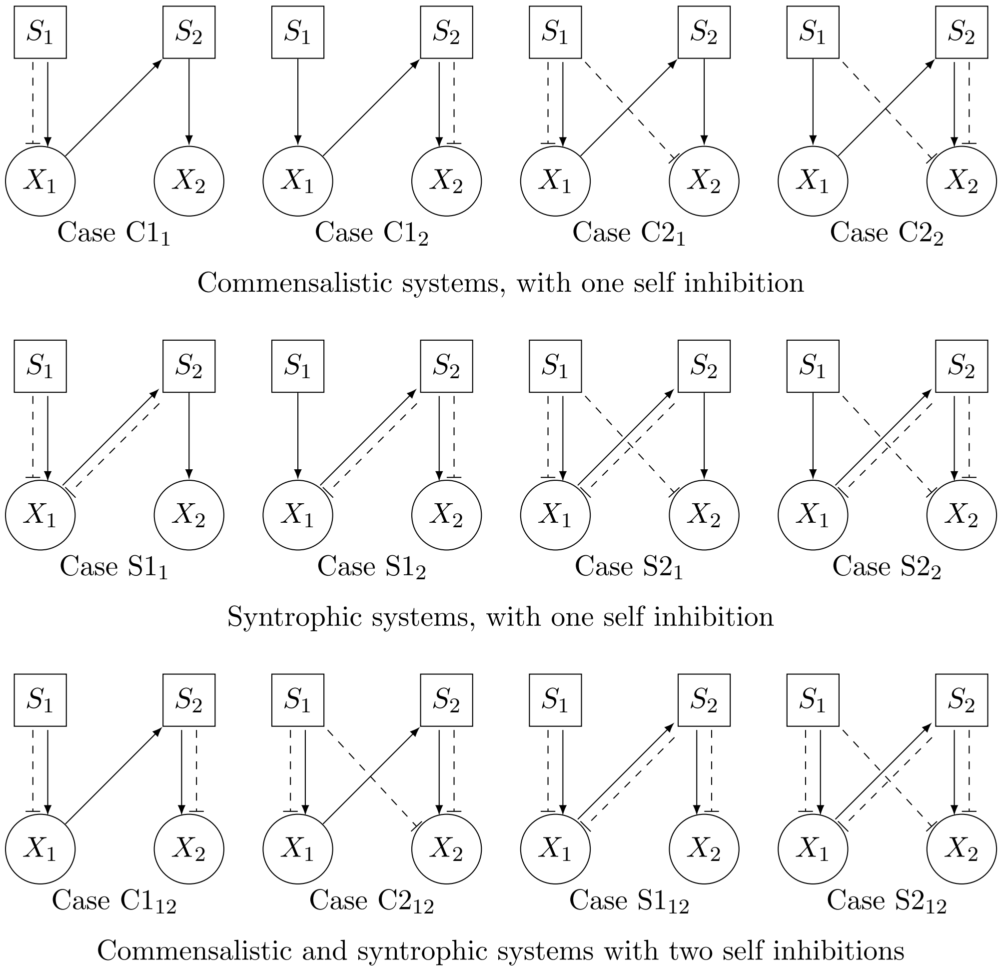

Figure 10: Commensalistic and syntrophic systems with self inhibition.

We assume that f_1 satisfies the following condition:

$$\text{For all } s_1 > 0,\ f_1'(s_1) > 0. \tag{4.2}$$

We assume that f_2 satisfies the following condition:

$$\text{There exists } s_2^m > 0 \text{ such that } f_2'(s_2) > 0 \text{ for } 0 < s_2 < s_2^m \text{ and } f_2'(s_2) < 0 \text{ for } s_2 > s_2^m. \tag{4.3}$$

The break-even concentrations $\lambda_1(D)$, $\lambda_2^1(D)$ and $\lambda_2^2(D)$, of (4.1), are defined by:

Definition 2. *Let $m_1 = f_1(+\infty) = \sup_{s_1>0} f_1(s_1)$. For $D \in [0, m_1)$, the break-even concentration is the unique solution $s_1 = \lambda_1(D)$ of equation $f_1(s_1) = D$.*
Let $m_2 = f_2(s_2^m) = \sup_{s_2>0} f_1(s_2)$. For $D \in [0, m_2)$, the break-even concentration are the solutions $\lambda_2^1(D)$ and $\lambda_2^2(D)$ of equation $f_2(s_2) = D$, such that $0 < \lambda_2^1(D) < s_2^m < \lambda_2^2(D) \leq +\infty$.

Note that for D close to m_2 we necessarily have two solutions, i.e. $0 < \lambda_2^1(D) < s_2^m < \lambda_2^2(D) < +\infty$. However, for D small enough, there may be only one solution, $\lambda_2^1(D)$, and the second solution $\lambda_2^2(D)$ does not

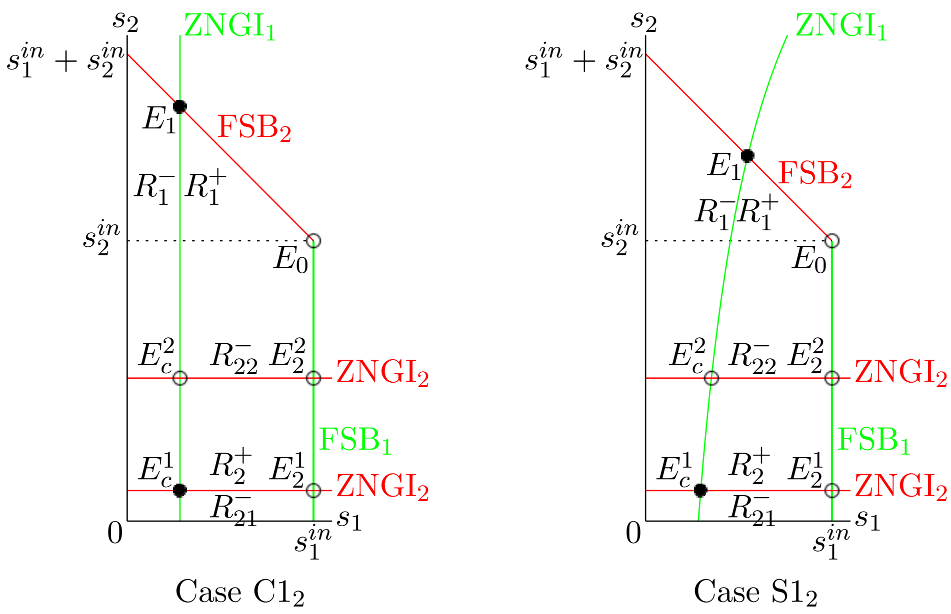

Figure 11: The feasible set and the ZNGIs for the commensalistic case C1$_2$ and the syntrophic case S1$_2$.

Table 5: Conditions of existence and stability of the equilibria of (4.1) or (4.5).

	Existence condition	Stability condition (local)
E_0	Always exists	$E_0 \in R_1^- \cap R_2^-$
E_1	$E_0 \in R_1^+$	$E_1 \in R_2^-$
E_2^1	$E_0 \in R_2^+ \cup \overline{R_{22}^-}$	$E_2^1 \in R_1^-$
E_2^2	$E_0 \in R_{22}^-$	Unstable if it exists
E_c^1	$E_c^1 \in \mathcal{F}^o$	Stable if it exists
E_c^2	$E_c^2 \in \mathcal{F}^o$	Unstable if it exists

exist. The ZNGIs of (4.1) are given by $\text{ZNGI}_1 = \left\{(s_1, s_2) \in \mathbb{R}_+^2 : s_1 = \lambda_1(D_1)\right\}$ and

$$\text{ZNGI}_2 = \left\{(s_1, s_2) \in \mathbb{R}_+^2 : s_2 = \lambda_2^1(D_2)\right\} \cup \left\{(s_1, s_2) \in \mathbb{R}_+^2 : s_2 = \lambda_2^2(D_2)\right\}. \tag{4.4}$$

Note that in this case, the R_2^- region has two connected components: $R_2^- = R_{21}^- \cup R_{22}^-$, where

$$R_{21}^- = \left\{(s_1, s_2) \in \mathbb{R}_+^2 : s_2 < \lambda_2^1(D_2)\right\}, \quad R_{22}^- = \left\{(s_1, s_2) \in \mathbb{R}_+^2 : s_2 > \lambda_2^2(D_2)\right\}.$$

Moreover, we have

$$R_2^+ = \left\{(s_1, s_2) \in \mathbb{R}_+^2 : \lambda_2^1(D_2) < s_2 < \lambda_2^2(D_2)\right\}.$$

What's new compared to the C1 case (see Fig 2, Case C1) is that, since ZNGI$_2$ has two components, we have a multiple crossing of ZNGI$_2$ with ZNGI$_1$ and ZNGI$_2$ with FSB$_1$. The system can have up to six equilibria, see Fig. 11. The existence and stability conditions of these equilibria are summarized in Table 5.

To construct the operating diagram, we consider

- the vertical line Γ_1 of equation $s_1^{in} = \lambda_1(D_1)$,

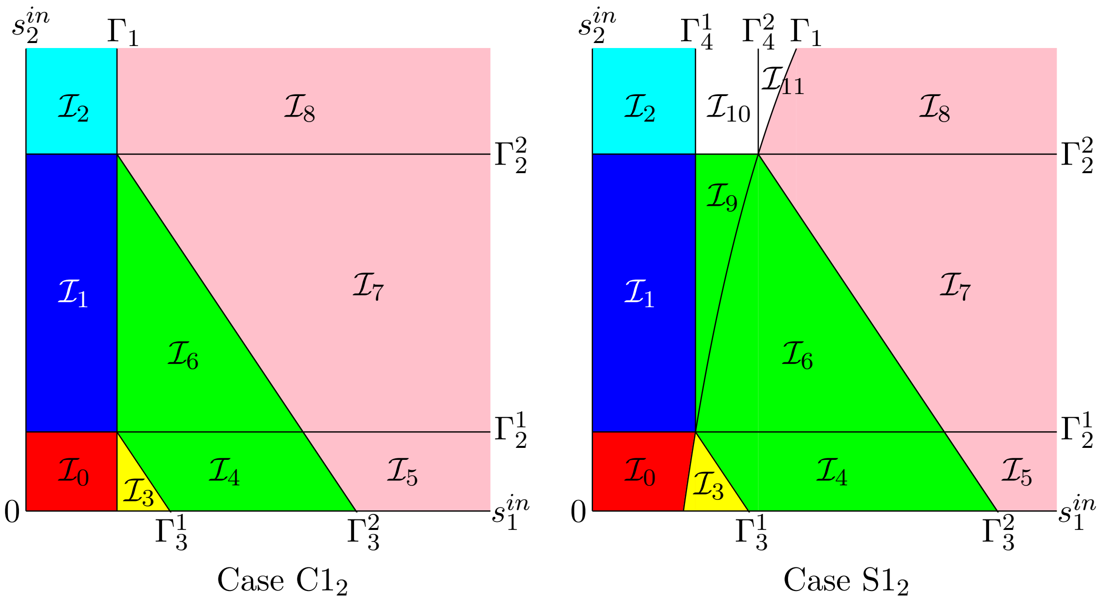

Figure 12: The operating diagram of (4.1) or (4.5) in the $\left(s_1^{in}, s_2^{in}\right)$ operating plane and $D \in (0, \delta_0)$. The existence and stability of the equilibria in the regions $\mathcal{I}_k$ are given in Table 6 for case $\mathrm{C}1_2$ and Table 7 for case $\mathrm{S}1_2$.

- the horizontal lines Γ_2^j of equations $s_2^{in} = \lambda_2^j(D_2)$, $j = 1, 2$,
- the oblique lines Γ_3^j of equations $s_1^{in} + s_2^{in} = \lambda_1(D_1) + \lambda_2^j(D_2)$, $j = 1, 2$.

These lines divide the set of operating parameters $\left(s_1^{in}, s_2^{in}\right)$ in nine regions denoted $\mathcal{I}_k$, $k = 0, \ldots, 8$, as depicted in Fig. 12 (Case $\mathrm{C}1_2$).

Proposition 7. *The conditions of existence and stability of the equilibria of (4.1) in the regions $\mathcal{I}_k$ of Fig. 12 (Case* $\mathrm{C}1_2$*) are given in Table 6.*

Proof. The proof is given in Fig. 13. Assume that $\left(s_1^{in}, s_2^{in}\right) \in \mathcal{I}_8$. We see in Fig. 13 that E_0 is unstable since $E_0 \notin R_1^- \cap R_2^-$, E_1 exists since $E_0 \in R_1^+$ and is stable since $E_1 \in R_2^-$, E_2^1 and E_2^2 exist since $E_0 \in R_{22}^-$ and E_2^1 is unstable since $E_2^1 \notin R_1^-$, E_c^1 and E_c^2 exist. The proofs for all other regions are similar. The proof for global asymptotic stability is given in Section B.1. □

For a more detailed study of the model $\mathrm{C}1_2$ and information on how the operating diagram changes when the biological parameters are changed, as well as operating diagrams in the operating plane $\left(s_1^{in}, D\right)$, where s_2^{in} is kept constant, the reader is referred to [8, 38].

4.3 Syntrophy with inhibition of the second species by its limiting substrate

We consider case $\mathrm{S}1_2$ in Fig. 10. The model takes the form

$$
\begin{aligned}
\dot{s}_1 &= D\left(s_1^{in} - s_1\right) - f_1(s_1, s_2)\, x_1, \\
\dot{x}_1 &= \left(f_1(s_1, s_2) - D_1\right) x_1, \\
\dot{s}_2 &= D\left(s_2^{in} - s_2\right) + f_1(s_1, s_2)\, x_1 - f_2(s_2)\, x_2, \\
\dot{x}_2 &= \left(f_2(s_2) - D_2\right) x_2.
\end{aligned}
\tag{4.5}
$$

Table 6: Existence and stability of equilibria of (2.5) in the regions of the operating diagram depicted in Fig. 12 (Case $C1_2$).

	E_0	E_2^1	E_2^2	E_1	E_c^1	E_c^2	Color
$\mathcal{I}_0$	GAS						Red
$\mathcal{I}_1$	U	GAS					Blue
$\mathcal{I}_2$	S	S	U				Cyan
$\mathcal{I}_3$	U			GAS			Yellow
$\mathcal{I}_4$	U			U	GAS		Green
$\mathcal{I}_5$	U			S	S	U	Pink
$\mathcal{I}_6$	U	U		U	GAS		Green
$\mathcal{I}_7$	U	U		S	S	U	Pink
$\mathcal{I}_8$	U	U	U	S	S	U	Pink

We assume that $f_1(s_1, s_2)$ and $f_2(s_2)$ satisfy (3.9) and (4.3), respectively.

The break-even concentrations $\lambda_1(s_2, D)$, $\lambda_2^1(D)$ and $\lambda_2^2(D)$, of (4.5), are defined by Definitions 1 and 2, respectively. The ZNGI$_1$ of (4.1) is given by ZNGI$_1$ = $\left\{(s_1, s_2) \in \mathbb{R}_+^2 : s_1 = \lambda_1(s_2, D_1)\right\}$, while ZNGI$_2$ is given by (4.4). As for the commensalistic case, the system can have up to six equilibria, see Fig. 11, whose conditions of existence and stability are also given by Table 5.

What's new compared to the $C1_2$ case is that the vertical line Γ_1 of the commensalistic model becomes now the curve of equation $s_1^{in} = \lambda_1\left(s_2^{in}, D_1\right)$. The horizontal lines Γ_2^j are not changed, and the oblique lines Γ_3^j have now equations $s_1^{in} + s_2^{in} = \lambda_1\left(\lambda_2^j(D_2), D_1\right) + \lambda_2^j(D_2)$, $j = 1, 2$. We must also consider the vertical lines Γ_4^j of equations $s_1 = \lambda_1\left(\lambda_2^j(D_2), D_1\right)$, $j = 1, 2$. All these lines divide the set of operating parameters $\left(s_1^{in}, s_2^{in}\right)$ in twelve regions denoted $\mathcal{I}_k$, $k = 0, \ldots, 11$, depicted in Fig. 12 (Case $S1_2$).

Table 7: Conditions of existence and stability of equilibria of (2.5) in the regions of the operating diagram depicted in Fig. 12 (Case $S1_2$).

	E_0	E_2^1	E_2^2	E_1	E_c^1	E_c^2	Color
$\mathcal{I}_0$	S						Red
$\mathcal{I}_1$	U	S					Blue
$\mathcal{I}_2$	S	S	U				Cyan
$\mathcal{I}_3$	U			S			Yellow
$\mathcal{I}_4$	U			U	S		Green
$\mathcal{I}_5$	U			S	S	U	Pink
$\mathcal{I}_6$	U	U		U	S		Green
$\mathcal{I}_7$	U	U		S	S	U	Pink
$\mathcal{I}_8$	U	U	U	S	S	U	Pink
$\mathcal{I}_9$	U	U			S		Green
$\mathcal{I}_{10}$	S	U	U		S		White
$\mathcal{I}_{11}$	S	U	U		S	U	White

Proposition 8. *The existence and stability of the equilibria of (4.5) in the regions $\mathcal{I}_k$, $k = 0, \ldots, 11$ of Fig. 12 (Case $S1_2$) are given in Table 7.*

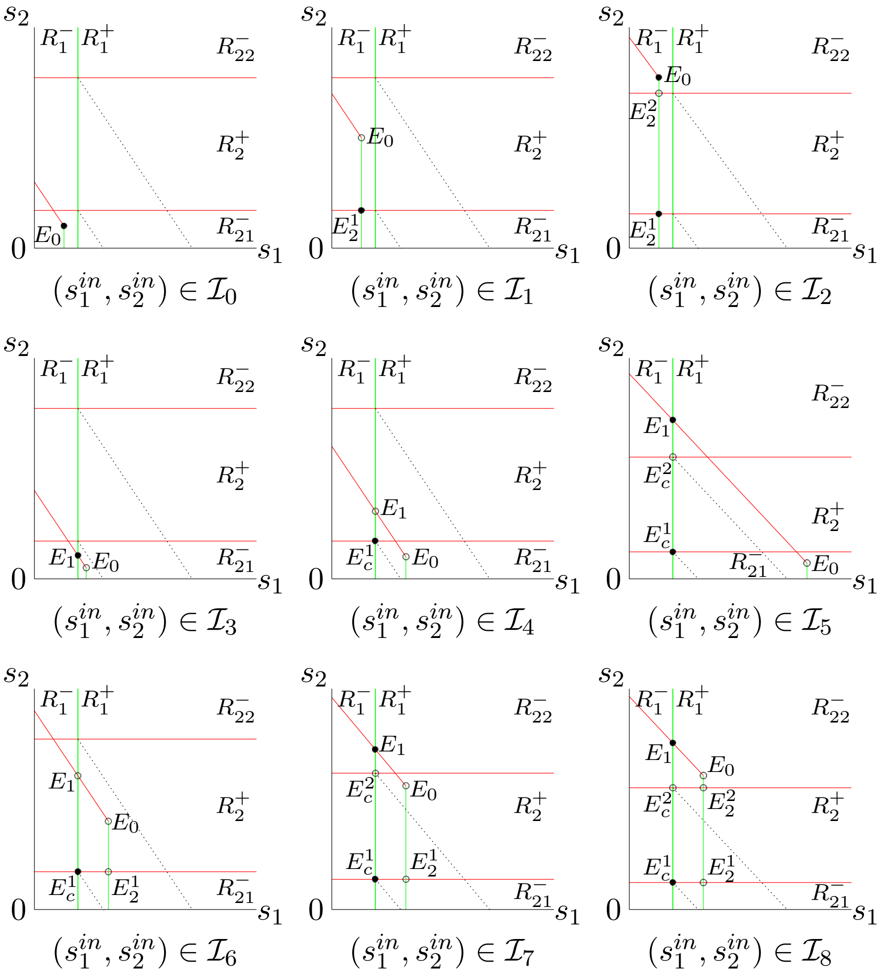

Figure 13: Proof of Proposition 7: feasible sets and ZNGIs, showing equilibria and their stability, for the nine regions of the operating diagram, shown in Fig.12 (Case C1_2).

Proof. The proof for the regions $\mathcal{I}_k$, $k = 0, \ldots, 8$ is the same as the proof of Proposition 7 and is given in Appendix D.4. The proof for the new regions $\mathcal{I}_k$, $k = 9, 10$ and 11, which do not exist in the commensalistic case, are given in Fig. 14. Assume that $\left(s_1^{in}, s_2^{in}\right) \in \mathcal{I}_{11}$. We see in Fig. 14 that E_0 is stable since $E_0 \in R_1^- \cap R_2^-$, E_1 does exist since $E_0 \notin R_1^+$, E_2^1 and E_2^2 exist since $E_0 \in R_{22}^-$ and E_2^1 is unstable since $E_2^1 \notin R_1^-$, E_c^1 and E_c^2 exist. The proofs for the other regions is similar. □

The most important novelty on the asymptotic behavior of S1_2 compared to C1_2 is the appearance of the white regions $\mathcal{I}_{10}$ and $\mathcal{I}_{11}$ of bistability of the washout equilibrium E_0 and the coexistence equilibrium E_c^1. For a more detailed study of the model S1_2 and information on how the operating diagram changes when the biological parameters are changed, as well as operating diagrams in the operating plane $\left(s_1^{in}, D\right)$, where s_2^{in} is kept constant, the reader is referred to [20].

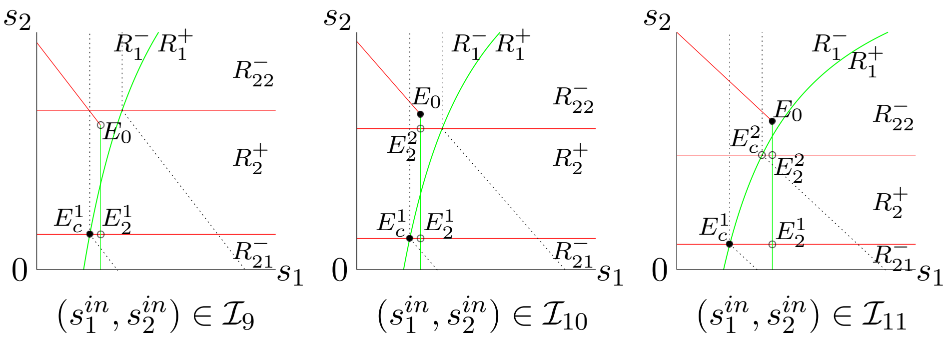

Figure 14: Proof of Proposition 8 in the regions $\mathcal{I}_k$, $k = 9, 10, 11$ of Fig.12 (Case $S1_2$).

5 Discussion

In this work we have studied the general model (2.5) of commensalism or syntrophy. This model contains a large number of models in the existing literature. The case where f_1 does not depend on s_2, or f_2 does not depend on s_1 were studied in the literature when the removal rates D_i are not equal to the dilution rate D, see [8, 15, 20, 40, 44]. However, the case where f_1 depends also on s_2, and f_2 depends also on s_1 were studied in the literature only when $D_1 = D_2 = D$, so that the system can be reduced to a planar system, see [39]. Our mathematical analysis of the model has revealed several possible behaviors: Proposition 3 provides a complete theoretical description of asymptotic behavior of the system. In order that the results can be useful in practice, one must have a description of the system with respect to the operating parameters. The study of bifurcations according to the operating parameters D, s_1^{in}, s_2^{in} is the most meaningful one for the laboratory model, since the experimenter can easily vary these parameters.

Our results contain all the results from the literature as special cases, and more importantly present them in a unified way. The advantage of this unified presentation is that it also shows the similarities between the models, and emphasizes the new behaviors that can emerge when new assumptions are introduced. For example

- Extending the model from Case C1 (i.e. $f_i(s_i)$ depends only on s_i, $i = 1, 2$) to Case C2 (i.e. $f_2(s_1, s_2)$ is allowed to depend on s_1 as well) introduces no new system behaviors: the same number of equilibria, the same asymptotic behaviors. The only modification is that the regions of the operating diagram are slightly modified, see Fig. 4 (Cases C1 and C2) and Table 2.

- However, extending the model from Case C1 to Case S1 (i.e. $f_1(s_1, s_2)$ is allowed to depend on s_2 as well) introduces new system behaviors: although the system retains the same number of equilibria, a new region appears in the operating diagram, see Fig. 4 (Case S1) and Table 3.

- On the other hand, extending the model from the C2 case to the S2 case (i.e. $f_1(s_1, s_2)$ is allowed to depend on s_2 as well and $f_2(s_1, s_2)$ is allowed to depend on s_1 as well) introduces the most novelties in the system's behavior, the most important being the possibility of multiple coexistence equilibria, as well as a variety of asymptotic system behavior, including bistability, see Fig. 7.

- When self-inhibition is allowed in the model, our graphical method makes it easy to compare the system's asymptotic behaviors and to highlight the contribution of syntrophy (case $S1_2$) versus commensalism (case $C1_2$). Figure 12 and Table 7 show how syntrophy brings out the possibility of bistability between the washout equilibrium E_0 and the coexistence equilibrium E_c^1 (see the white regions). This bistability does not occur in the commensal (case $C1_2$) model, as shown in Figure 12 and Table 6.

In the case without self-inhibition, the bistability phenomenon necessarily requires that the function f_1 depends on s_2 and the function f_2 depends on s_2. Indeed, the bistability of a positive equilibrium and a boundary equilibrium, where one of the species (or both) is extinct is possible only for the S2 model and not for the S1, C1 or C2 models. If one of the species is unaffected by the food of its partner, the system is unable to undergo bistability.

The growth functions KB1 and KB2 of Kreikenbohm and Bohl [28, 29], do not satisfy our assumptions since they are not C^1 but only piecewise C^1, see Table 14. I should be interesting to extend our graphical method to those cases. Moreover, the KB1 or KB2 functions are identically 0 until a threshold value and then become positive. Such function often appear in the biological literature since the growth of a species requires that the limiting substrate exceeds a certain threshold. The extension of our method in these cases, as well as in the cases with inhibitions between species (see Remark 1), will be considered in a future work.

A Operating diagrams where s_2^{in} is kept constant

In order that the results can be useful in practice, one must construct the operating parameter when the dilution rate D is varied because this operating parameter is the most commonly used control parameter in laboratories. Since s_1^{in} is the inlet concentration of the substrate of the overall system, a useful representation is to keep constant the inlet concentration s_2^{in} of the substrate s_2 produced by the first reaction and to describe the operating diagram in the operating plane $\left(s_1^{in}, D\right)$. The effects of s_2^{in} are shown in a series of operating diagrams. The construction of this diagram can be easily deduced from the construction of the operating diagram in the operating plane $\left(s_1^{in}, s_2^{in}\right)$ and D is kept fixed. The study carried out in the plane $\left(s_1^{in}, s_2^{in}\right)$ showed the existence of regions such that the system behaves in a certain way when the operating parameters are chosen in these regions. It is then sufficient to see how the boundaries of these regions, i.e. the Γ_i and Γ_i^j curves, are written in the operating plane $\left(s_1^{in}, D\right)$ and which regions of this plane they delimit. In the following sections we illustrate this construction in models C1, C2 and S1 as well as in a typical example of model S2.

A.1 Commensalism and pure syntrophy

Fig. 15 shows the regions $\mathcal{I}_k$, previously identified in Fig. 4, in the operating plane (s_1^{in}, D), where s_2^{in} is kept constant. The number of regions depends on s_2^{in}. Let us describe the operating diagram in the case $\delta_1 > \delta_2$, where δ_1 and δ_2 are defined by (3.16). The case $\delta_1 \le \delta_2$ is similar and is left to the reader.

Note that for C1, Γ_1 is the curve of equation $D = \left(f_1\left(s_1^{in}\right) - a_1\right)/\alpha_1$ and Γ_2 is the horizontal line of equation $D = \left(f_2\left(s_2^{in}\right) - a_2\right)/\alpha_2$, which is not empty if and only if $s_2^{in} > \lambda_2(a_2)$. On the other hand Γ_3 is the curve of equation $s_1^{in} + s_2^{in} = \lambda_1(D_1) + \lambda_2(D_2)$. The novelty when we consider model C2 is that Γ_2 becomes the curve of equation $f_2\left(s_1^{in}, s_2^{in}\right) = D_2$. This curve is not empty if and only if $f_2(0, s_2^{in}) > a_2$ which is equivalent to $s_2^{in} > \lambda_2(0, a_2)$. The novelty when we consider model S1 is that the curve Γ_1 becomes the curve of equation $s_1^{in} = \lambda_1\left(s_2^{in}, D_1\right)$, and is therefore distinct from Γ_4, which is the curve of equation $s_1^{in} = \lambda_1(\lambda_2(D_2), D_1)$. For the study of the intersection point of Γ_i curves of the model C2, we need to define the following function

$$D \in (0, \delta_2) \mapsto \xi(D) := \lambda_2(\lambda_1(D_1), D_2).$$

Using (3.9) and (3.10) we see that $\xi'(D) > 0$. Hence, ξ is an increasing function from $\xi(0) = \lambda_2(\lambda_1(a_1), a_2)$ to

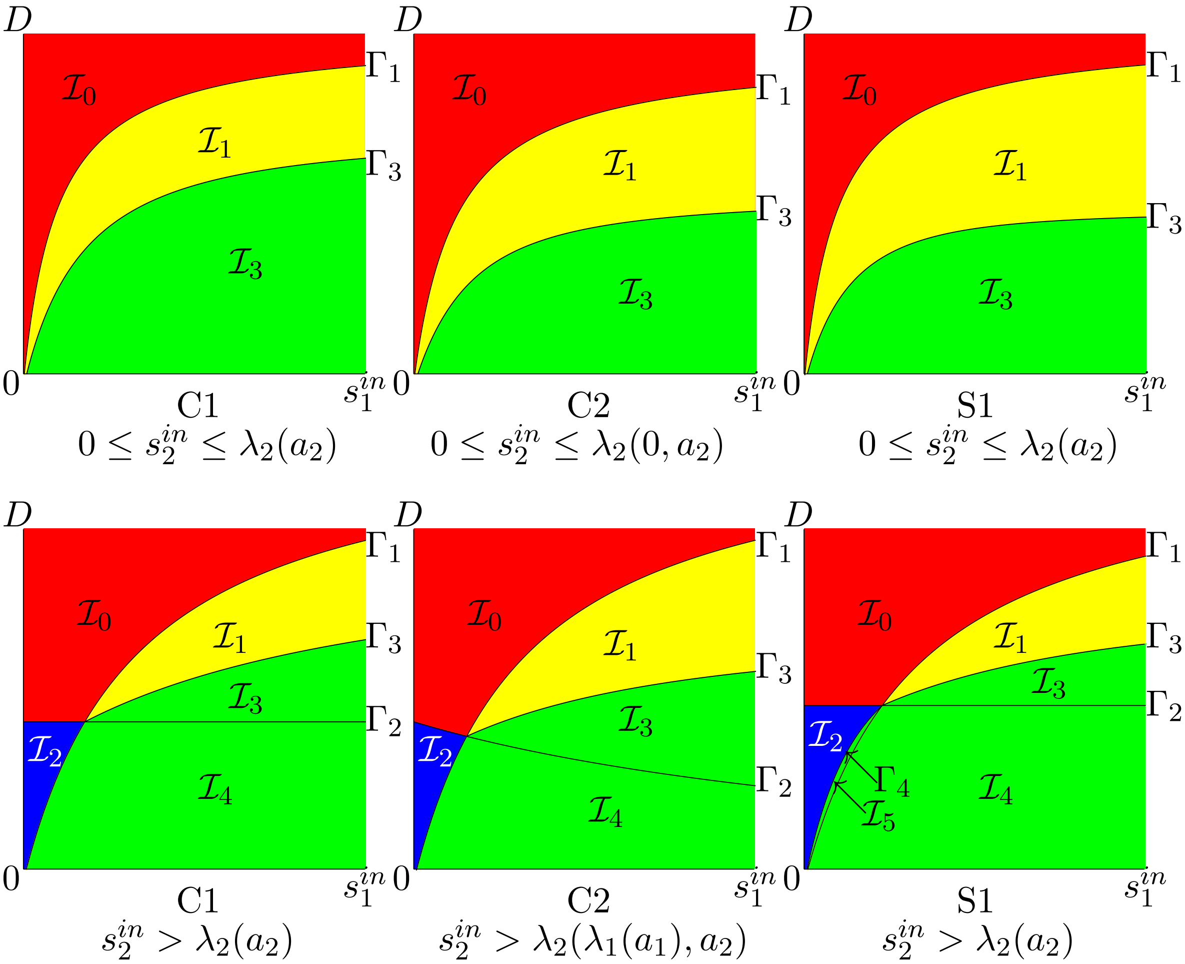

Figure 15: The operating diagram of Cases C1, C2 and S1, in the operating plane $\left(s_1^{in}, D\right)$, when $\delta_1 > \delta_2$, where δ_i are defined by (3.16).

$\xi(\delta_2) = +\infty$. It then has an inverse function ξ^{-1}. The curves Γ_i intersect at $P\left(s_2^{in}\right)$ defined by

$$P\left(s_2^{in}\right) = \begin{cases} (\lambda_1(\alpha_1 D_0 + a_1), D_0) & \text{where } D_0 = \frac{f_2\left(s_2^{in}\right) - a_2}{\alpha_2} & \text{for model C1,} \\ (\lambda_1(\alpha_1 D_0 + a_1), D_0) & \text{where } D_0 = \xi^{-1}\left(s_2^{in}\right) & \text{for model C2,} \\ \left(\lambda_1\left(s_2^{in}, \alpha_1 D_0 + a_1\right), D_0\right) & \text{where } D_0 = \frac{f_2\left(s_2^{in}\right) - a_2}{\alpha_2} & \text{for model S1.} \end{cases}$$

Therefore, for C1 and $s_2^{in} > \lambda_2(a_2)$, the five regions $\mathcal{I}_k$, $k = 0, \ldots, 4$, appear as shown in Fig. 15. Similarly for C2 and $s_2^{in} > \lambda_2(\lambda_1(a_1), a_2)$, the five regions $\mathcal{I}_k$ appear, while for S1 and $s_2^{in} > \lambda_2(a_2)$, the sixth region $\mathcal{I}_5$ appears, see Fig. 15 (Case S1).

If $0 \leq s_2^{in} \leq \lambda_2(a_2)$, for models C1 and S1, only the $\mathcal{I}_0$, $\mathcal{I}_1$ and $\mathcal{I}_3$ regions appear, as it is depicted in Fig. 15 (Cases C1 and S1). For C2 two cases must be distinguished: If $0 \leq s_2^{in} \leq \lambda_2(0, a_2)$, only the $\mathcal{I}_0$, $\mathcal{I}_1$ and $\mathcal{I}_3$ regions appear, in Fig. 15 (Case C2). If $\lambda_2(0, a_2) < s_2^{in} \leq \lambda_2(\lambda_1(a_1), a_2)$, a small $\mathcal{I}_2$ region also appears, close to the origin, as shown in Fig. 16.

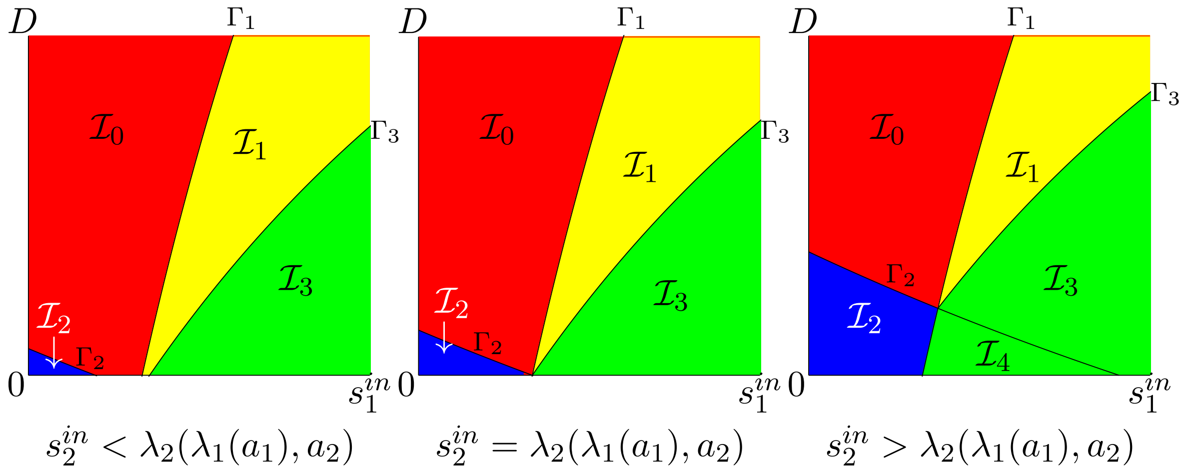

Figure 16: An enlargement near the origin of the operating diagram in Fig. 15 (Case C2), showing the appearance of the $\mathcal{I}_2$ region, when $s_2^{in} > \lambda_2(0, a_2)$.

A.2 An illustrative example in the S2 case

We consider the model S2 of Table 1. The curves Γ_1, Γ_2, Γ_3^i and Γ_4^i, $i = 1, 2$, which are the boundaries of the various regions have been derived analytically. Indeed, since s_2^{in} is kept fixed, and using (2.2), we have the following equations for these curves

- Γ_1 is the curve of equation $D = \frac{f_1(s_1^{in}, s_2^{in}) - a_1}{\alpha_1}$.
- Γ_2 is the curve of equation $D = \frac{f_2(s_1^{in}, s_2^{in}) - a_2}{\alpha_2}$.
- Γ_3^i and Γ_4^i, $i = 1, 2$, as defined by (3.17), are also curves in the operating plane $\left(s_1^{in}, D\right)$.

In addition to these curves we must also consider the horizontal line defined by

$$\Gamma_0 = \left\{\left(s_1^{in}, D\right) \in \mathbb{R}_+^2 : D = \delta_0\right\}, \tag{A.1}$$

where δ_0 is the value of D for which the ZNGIs are tangent, see Assumption **H3** and Fig. 9. These curves divide the operating plane (s_1^{in}, D) in nine regions, corresponding to the nine regions depicted in Figs. 7 and 9. Therefore, the operating diagrams can be drawn by plotting all these curves.

It is not possible to give a general qualitative description of the operating diagram as we did in Section 3.2.1 for models C1, C2 and S1. In Figs. 17 and 18 we present the specific example given in Table 4. Increasing s_2^{in} from $s_2^{in} = 0$ to $s_2^{in} = 7$, we draw the curves Γ_j, $j = 0, 1, 2$, Γ_3^i and Γ_4^i, $i = 1, 2$, and color the $\mathcal{I}_k$ regions they delimit, with the colors already used in Fig. 7.

We explain briefly how these figures are obtained. For $s_2^{in} = 0$, curves Γ_2, Γ_4^1 and Γ_4^2 are empty and only regions $\mathcal{I}_0$, $\mathcal{I}_1$, $\mathcal{I}_3$ and $\mathcal{I}_6$ appear, as shown in the panel $s_2^{in} = 0$ in Fig. 17. When $s_2^{in} = 1$, curves Γ_2, Γ_4^1 are not empty and regions $\mathcal{I}_2$, $\mathcal{I}_4$ and $\mathcal{I}_5$ also appear. See the panel $s_2^{in} = 1$, and its enlargement, in Fig. 17. If s_2^{in} is increased to $s_2^*(\delta_0)$, corresponding to the tangency of the ZNGIs, then no new region appears. If s_2^{in} is increased further, then curve Γ_4^2 appears, while curve Γ_3^1 disappears, defining two new regions $\mathcal{I}_7$ and $\mathcal{I}_8$. Therefore the nine regions of the operating diagram in Fig. 7 appear. See the panel $s_2^{in} = 4$, and its

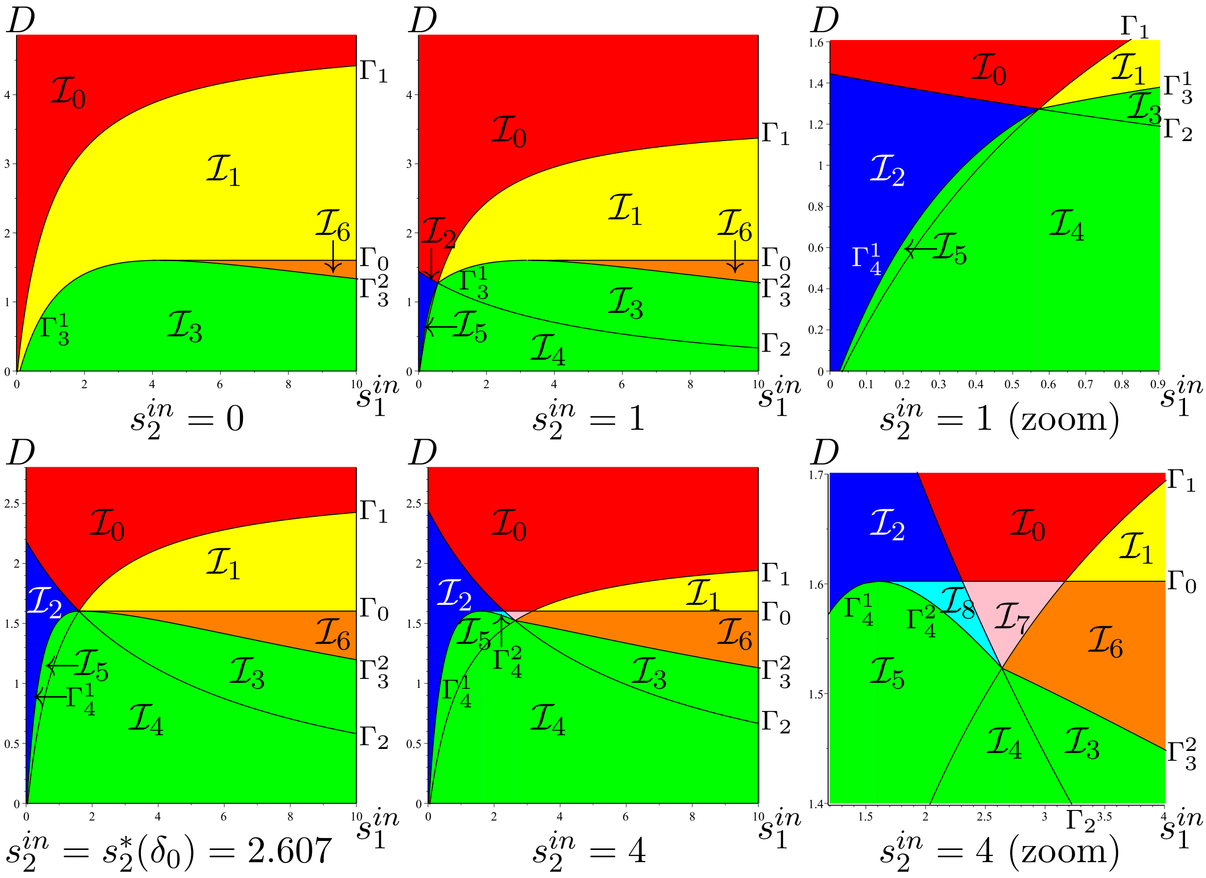

Figure 17: The operating diagram of (2.5), for the growth functions given in Table 4, in the (s_1^{in}, D) operating plane, with s_2^{in} kept constant.

enlargement, in Fig. 17 and the panel $s_2^{in} = 5$, in Fig. 18. If s_2^{in} is increased to $s_2^{in} = 6.315$, then the nine regions continue to appear. The value $s_2^{in} = 6.315$ corresponds to the tangency of curves Γ_0 and Γ_1 and is given by equation $f_1(+\infty, s_2^{in}) = \alpha_1\delta_0 + a_1$. If s_2^{in} is increased further, then the region $\mathcal{I}_1$ disappears, see the panel $s_2^{in} = 7$ in Fig. 18.

B Global results

The local stability analysis only implies that the solutions starting near an asymptotically stable equilibrium converge toward this equilibrium. Hence one cannot make assertions about the eventual outcome that are global in the sense that they are independent of the initial conditions. However, in some cases one can reduce the four-dimensional system (2.5) to a two-dimensional system, whose global study is in general more easy. Thanks to Thieme's theory [48, 49], we can deduce the global asymptotic stability of the initial four-dimensional system from the global asymptotic stability of the reduced two-dimensional one. For details and complements, on how to use Thieme's theory, see [23, Appendix A] or [45, Appendix F]. This reduction

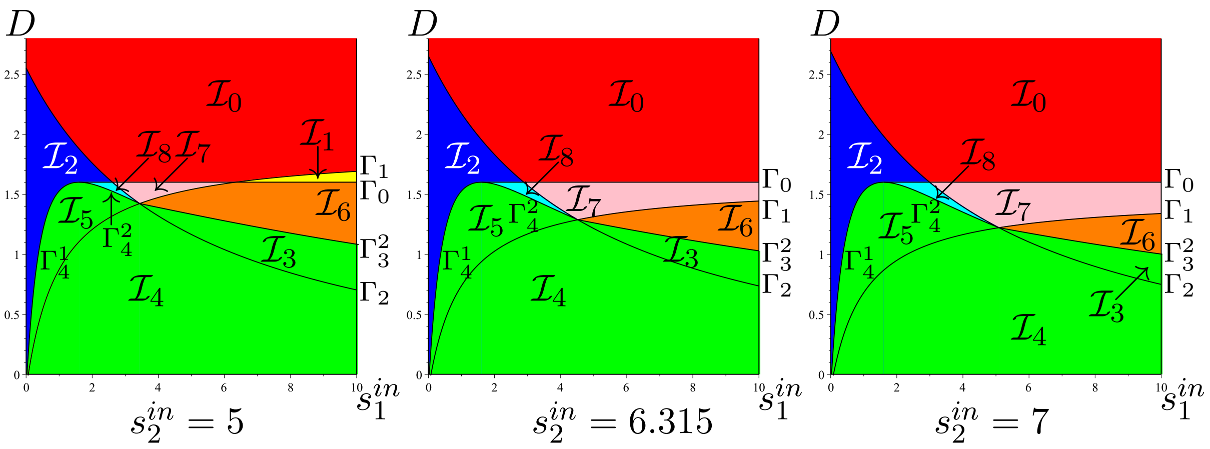

Figure 18: The operating diagram of (2.5), for the growth functions given in Table 4, in the $\left(s_1^{in}, D\right)$ operating plane, with s_2^{in} kept constant.

is possible for the commensalistic models in the general case when the removal rates are not equal to the dilution rate and also in the syntrophic models when they are (i.e. $D_1 = D_2 = D$).

B.1 Commensalism

We consider the commensalistic model C2_{12} in Fig. 10. The system (2.5) becomes

$$\begin{array}{rcl} \dot{s}_1 & = & D\left(s_1^{in} - s_1\right) - f_1\left(s_1\right)x_1, \\ \dot{x}_1 & = & \left(f_1\left(s_1\right) - D_1\right)x_1, \\ \dot{s}_2 & = & D\left(s_2^{in} - s_2\right) + f_1\left(s_1\right)x_1 - f_2\left(s_1, s_2\right)x_2, \\ \dot{x}_2 & = & \left(f_2\left(s_1, s_2\right) - D_2\right)x_2, \end{array} \tag{B.1}$$

where f_1 is not assumed to be necessarily increasing in s_1 and similarly f_2 is not assumed to be necessarily increasing in s_2. This system contains all commensalistic models C1, C2, C1_1, C1_2, C2_1, C2_2 and C1_{12}, as particular cases. For example C1_2 is obtained when f_1 satisfies (4.2) and f_2 depends only on s_2 and satisfies (4.3). The important thing is that system (B.1) has a cascade structure. Indeed, if $(s_1(t), x_1(t), s_2(t), x_2(t))$ is a solution of (B.1), then $(s_1(t), x_1(t))$ is a solution of the two-dimensional system

$$\begin{array}{rcl} \dot{s}_1 & = & D\left(s_1^{in} - s_1\right) - f_1\left(s_1\right)x_1, \\ \dot{x}_1 & = & \left(f_1\left(s_1\right) - D_1\right)x_1, \end{array} \tag{B.2}$$

and $(s_2(t), x_2(t))$ is a solution of the non autonomous two-dimensional system

$$\begin{array}{rcl} \dot{s}_2 & = & D\left(s_2^{in} - s_2\right) + f_1\left(s_1(t)\right)x_1(t) - f_2\left(s_1(t), s_2\right)x_2, \\ \dot{x}_2 & = & \left(f_2\left(s_1(t), s_2\right) - D_2\right)x_2. \end{array} \tag{B.3}$$

The system (B.2) is a classical chemostat system. Every solution (except for a set of initial conditions of measure 0) converges toward an equilibrium $\left(s_1^*, x_1^*\right)$, possibly the washout equilibrium $\left(s_1^{in}, 0\right)$. Therefore, the system (B.3) is an asymptotically autonomous system whose limiting system is

$$\begin{array}{rcl} \dot{s}_2 & = & D\left(s_2^{in} - s_2\right) + f_1\left(s_1^*\right)x_1^* - f_2\left(s_1^*, s_2\right)x_2, \\ \dot{x}_2 & = & \left(f_2\left(s_1^*, s_2\right) - D_2\right)x_2. \end{array} \tag{B.4}$$

The system (B.4) is also a classical chemostat system and its solutions (except for a set of initial conditions of measure 0) converge toward an equilibrium $\left(s_2^*, x_2^*\right)$. Using Thieme's theory we can conclude on the global asymptotic stability of the system (B.1). This proves the global asymptotic behavior shown in Tables 2 and 6. For details and complements on how these kinds of arguments are conducted the reader is referred to [8, 38] for the $C1_2$ case in Fig. 10.

B.2 Syntrophy with the same removal rates

In this section, we consider the case where $D_1 = D_2 = D$. The system (2.5) becomes

$$\begin{array}{rcl} \dot{s}_1 & = & D\left(s_1^{in} - s_1\right) - f_1\left(s_1, s_2\right)x_1, \\ \dot{x}_1 & = & \left(f_1\left(s_1, s_2\right) - D\right)x_1, \\ \dot{x}_2 & = & \left(f_2\left(s_1, s_2\right) - D\right)x_2, \\ \dot{s}_2 & = & D\left(s_2^{in} - s_2\right) + f_1\left(s_1, s_2\right)x_1 - f_2\left(s_1, s_2\right)x_2, \end{array} \tag{B.5}$$

We consider the change of variables defined by

$$z_1 = s_1 + x_1, \quad z_2 = s_2 - x_1 + x_2. \tag{B.6}$$

The system (B.5) becomes

$$\begin{array}{rcl} \dot{x}_1 & = & \left(f_1\left(z_1 - x_1, z_2 + x_1 - x_2\right) - D\right)x_1, \\ \dot{x}_2 & = & \left(f_2\left(z_1 - x_1, z_2 + x_1 - x_2\right) - D\right)x_2, \\ \dot{z}_1 & = & D\left(s_1^{in} - z_1\right), \\ \dot{z}_2 & = & D\left(s_2^{in} - z_2\right). \end{array} \tag{B.7}$$

Since $z_1(t)$ and $z_2(t)$ exponentially converge toward s_1^{in} and s_2^{in} respectively, (B.7) is an asymptotically autonomous system, whose limiting system is

$$\begin{array}{rcl} \dot{x}_1 & = & \left(\phi_1(x_1, x_2) - D\right)x_1, \\ \dot{x}_2 & = & \left(\phi_2(x_1, x_2) - D\right)x_2, \end{array} \tag{B.8}$$

where ϕ_1 and ϕ_2 are defined by

$$\phi_1(x_1, x_2) = f_1\left(s_1^{in} - x_1, s_2^{in} + x_1 - x_2\right), \quad \phi_2(x_1, x_2) = f_2\left(s_1^{in} - x_1, s_2^{in} + x_1 - x_2\right).$$

Using Thieme's theory, the asymptotic behaviour of the solutions of the reduced model (B.8) is informative for the complete system (B.7). For details and complements on how these kinds of arguments are conducted the reader is referred to [39] for the S2 model, when $D_1 = D_2 = D$.

C Bifurcation diagrams

Along Γ_0, defined by (A.1), i.e. when $D = \delta_0$, a saddle-node bifurcation, in which E_c^1 and E_c^2 collide and annihilate each other, can occur, see Figs. 9, 17 and 18. The transcritical bifurcations occurring along Γ_1, Γ_2, Γ_3^j and Γ_4^j, $j = 1, 2$, are summarized in Table 8. The result is a straightforward consequence of Proposition 3.

Table 8: Codimension-one bifurcations of equilibria along the boundaries of the $\mathcal{I}_k$ regions. Only transcritical bifurcations (TB) and saddle-node bifurcations (SNB) occur.

Boundary	Bifurcation
$\Gamma_0 = \left(\overline{\mathcal{I}_1} \cap \overline{\mathcal{I}_6}\right) \bigcup \left(\overline{\mathcal{I}_2} \cap \overline{\mathcal{I}_8}\right) \bigcup \left(\overline{\mathcal{I}_0} \cap \overline{\mathcal{I}_7}\right)$	$E_c^1 = E_c^2$ (SNB)
$\Gamma_1 = \left(\overline{\mathcal{I}_0} \cap \overline{\mathcal{I}_1}\right) \bigcup \left(\overline{\mathcal{I}_4} \cap \overline{\mathcal{I}_5}\right) \bigcup \left(\overline{\mathcal{I}_6} \cap \overline{\mathcal{I}_7}\right)$	$E_0 = E_1$ (TB)
$\Gamma_2 = \left(\overline{\mathcal{I}_0} \cap \overline{\mathcal{I}_2}\right) \bigcup \left(\overline{\mathcal{I}_3} \cap \overline{\mathcal{I}_4}\right) \bigcup \left(\overline{\mathcal{I}_7} \cap \overline{\mathcal{I}_8}\right)$	$E_0 = E_2$ (TB)
$\Gamma_3^1 = \overline{\mathcal{I}_1} \cap \overline{\mathcal{I}_3}$	$E_1 = E_c^1$ (TB)
$\Gamma_3^2 = \overline{\mathcal{I}_3} \cap \overline{\mathcal{I}_6}$	$E_1 = E_c^2$ (TB)
$\Gamma_4^1 = \overline{\mathcal{I}_2} \cap \overline{\mathcal{I}_5}$	$E_2 = E_c^1$ (TB)
$\Gamma_4^2 = \overline{\mathcal{I}_5} \cap \overline{\mathcal{I}_8}$	$E_2 = E_c^2$ (TB)

We illustrate bifurcations by constructing in Fig. 19 the one-parameter bifurcation diagram, showing the equilibria as a function of parameter D, when s_1^{in} and s_2^{in} are fixed. We use the growth functions given in Table 4 and take $s_1^{in} = 10$, while the value for s_1^{in} is given in the figure. The behavior of the system is easily deduced from the operating diagrams shown in Figs. 17 and 18. Indeed, it corresponds to the behavior on the vertical line $s_1^{in} = 10$ of these diagrams. For example, if we take $s_2^{in} = 4$ we see in Fig. 17 (panel $s_2^{in} = 4$) that there exist four bifurcation values, $d_0 < d_1 < d_2 < d_3$ such that:

- If $D > d_3$, then $\left(s_1^{in} = 10, D\right) \in \mathcal{I}_0$. Hence, E_0 is the only equilibrium and is stable.
- If $d_3 > D > d_2$, then $\left(s_1^{in} = 10, D\right) \in \mathcal{I}_1$. Hence, E_0 and E_1 are the only equilibria, E_1 is stable and E_0 unstable.
- At $D = d_3$ a transcritical bifurcation occurs, in which E_0 and E_1 collide and exchange stability.
- If $d_2 > D > d_1$, then$\left(s_1^{in} = 10, D\right) \in \mathcal{I}_6$. Hence, E_0, E_1, E_c^1 and E_c^2 are the equilibria, E_1 and E_c^1 are stable, E_0 and E_c^2 are unstable.
- At $D = d_2$, a saddle-node bifurcation occurs, in which E_c^1 and E_c^2 collide and annihilate.
- If $d_1 > D > d_0$, then $\left(s_1^{in} = 10, D\right) \in \mathcal{I}_3$. Hence, E_0, E_1 and E_c^1 are the only equilibria, E_c^1 is stable, E_0 and E_1 are unstable.
- At $D = d_1$ a transcritical bifurcation occurs, in which E_1 and E_c^2 collide and E_1 becomes unstable.
- If $d_0 > D > 0$, then $\left(s_1^{in} = 10, D\right) \in \mathcal{I}_4$. Hence E_0, E_1, E_2 and E_c^1 are the equilibria, E_c^1 is stable, E_0, E_1 and E_2 are unstable.
- At $D = d_0$ a transcritical bifurcation occurs, in which E_2 and E_0 collide and E_2 disappears.

D Proofs

D.1 Proof of Proposition 3

Recall that an equilibrium is said to be stable if it is locally exponentially stable, i.e. the Jacobian matrix has eigenvalues with strictly negative real parts. We begin by proving the following result.

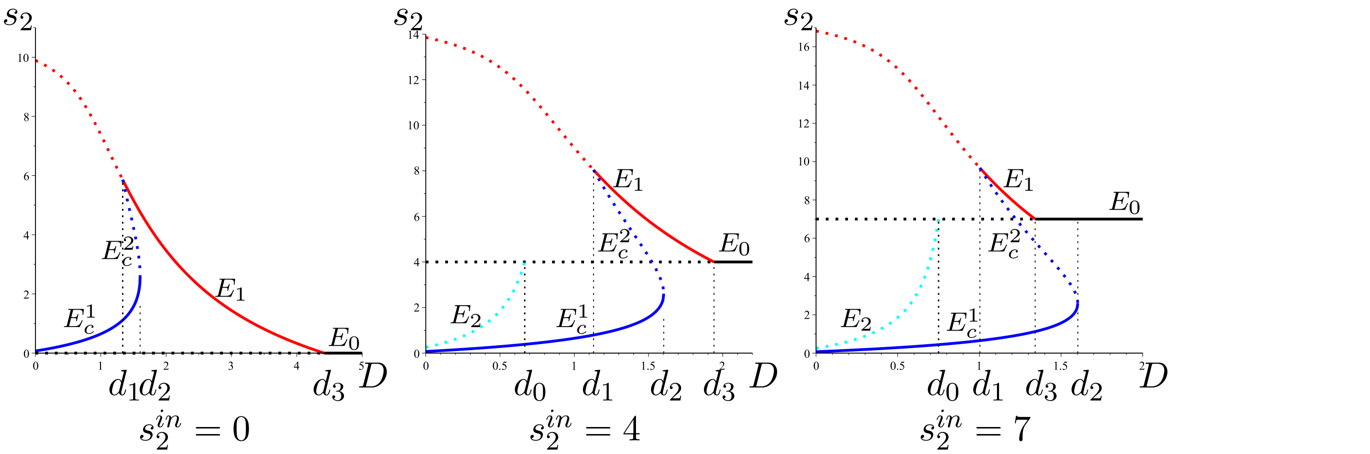

Figure 19: The bifurcation diagram of (2.5), showing the s_2-component of the equilibria, as a function of D, for the growth functions given in Table 4 and $s_1^{in} = 10$. An equilibrium is drawn in bold line when it is stable and in dotted line when it is unstable. Here $d_2 = \delta_0 \approx 1.602$. For $s_2^{in} = 0$, we have $d_1 \approx 1.335$ and $d_3 \approx 4.420$. For $s_2^{in} = 4$, we have $d_0 = 2/3$, $d_1 \approx 1.130$ and $d_3 \approx 1.941$. For $s_2^{in} = 7$, we have $d_0 = 0.75$, $d_1 \approx 1.002$ and $d_3 \approx 1.341$.

Proposition 9. *The system (2.5) can have four types of equilibria:*

1) The washout equilibrium $E_0 = (s_1^{in}, 0, s_2^{in}, 0)$, which always exists. It is stable if and only if

$$f_1\left(s_1^{in}, s_2^{in}\right) < D_1 \text{ and } f_2\left(s_1^{in}, s_2^{in}\right) < D_2. \tag{D.1}$$

2) A boundary equilibrium $E_1 = (\bar{s}_1, \bar{x}_1, \bar{s}_2, 0)$, where $\bar{s}_1$ is a solution of equation

$$f_1\left(s_1, s_1^{in} + s_2^{in} - s_1\right) = D_1, \tag{D.2}$$

and

$$\bar{s}_2 = s_1^{in} + s_2^{in} - \bar{s}_1, \quad \bar{x}_1 = \tfrac{D}{D_1}\left(s_1^{in} - \bar{s}_1\right). \tag{D.3}$$

It is unique if it exists. It exists if and only if

$$f_1\left(s_1^{in}, s_2^{in}\right) > D_1. \tag{D.4}$$

It is stable if and only if

$$f_2(\bar{s}_1, \bar{s}_2) < D_2. \tag{D.5}$$

3) A boundary equilibrium $E_2 = (\tilde{s}_1, 0, \tilde{s}_2, \tilde{x}_2)$, where

$$\tilde{s}_1 = s_1^{in}, \quad \tilde{s}_2 = \lambda_2\left(s_1^{in}, D_2\right), \quad \tilde{x}_2 = \tfrac{D}{D_2}\left(s_2^{in} - \tilde{s}_2\right). \tag{D.6}$$

It exists if and only if

$$f_2\left(s_1^{in}, s_2^{in}\right) > D_2. \tag{D.7}$$

It is stable if and only if

$$f_1(\tilde{s}_1, \tilde{s}_2) < D_1. \tag{D.8}$$

4) Coexistence equilibria $E_c = \left(s_1^*, x_1^*, s_2^*, x_2^*\right)$, where (s_1^*, s_2^*) is a solution of the system of equations

$$f_1(s_1, s_2) = D_1, \quad f_2(s_1, s_2) = D_2, \tag{D.9}$$

and

$$x_1^* = \tfrac{D}{D_1}\left(s_1^{in} - s_1^*\right), \quad x_2^* = \tfrac{D}{D_2}\left(s_1^{in} + s_2^{in} - s_1^* - s_2^*\right). \tag{D.10}$$

It exists if and only if $(s_1^*, s_2^*) \in \mathcal{F}^o$. *It is stable if and only if*

$$(f_{11}f_{22} - f_{12}f_{21})(s_1^*, s_2^*) > 0. \tag{D.11}$$

Proof. We begin by proving the conditions for the existence of equilibria. Using Lemma 2, for a boundary equilibrium $E_1 = (\bar{s}_1, \bar{x}_1, \bar{s}_2, 0)$, we have $(\bar{s}_1, \bar{s}_2) = \mathrm{ZNGI}_1 \cap \mathrm{FSB}_2$. This condition is equivalent to

$$f_1(\bar{s}_1, \bar{s}_2) = D_1 \quad \text{and} \quad \bar{s}_1 + \bar{s}_2 = s_1^{in} + s_2^{in}. \tag{D.12}$$

From the second formula in (D.12), we have $\bar{s}_2 = s_1^{in} + s_2^{in} - \bar{s}_1$, which is the first formula in (D.3). Replacing $\bar{s}_2$ in the first formula of (D.12), we have $f_1(\bar{s}_1, s_1^{in} + s_2^{in} - \bar{s}_1) = D_1$. Therefore, $\bar{s}_1$ is a solution of equation (D.2). The x_1 component is given then by (3.1), which proves the second formula in (D.3). The equation (D.2) is equivalent to $\psi_1(s_1) = D_1$, where $\psi_1(s_1) = f_1(s_1, s_1^{in} + s_2^{in} - s_1)$. We have

$$\psi_1'(s_1) = (f_{11} - f_{12})(s_1, s_1^{in} + s_2^{in} - s_1).$$

Using (3.9) we have $\psi_1'(s_1) > 0$ for all $s_1 > 0$. Therefore, equation (D.2) has at most one solution. Hence, if it exists, E_1 is unique. E_1 exists if and only if equation $\psi_1(s_1) = D_1$ has a solution in the interval $\left(0, s_1^{in}\right)$. Since $\psi_1(0) = 0$ and $\psi_1\left(s_1^{in}\right) = f_1\left(s_1^{in}, s_2^{in}\right)$, the solution exists if and only if $f_1\left(s_1^{in}, s_2^{in}\right) > D_1$, which proves (D.4).

Using Lemma 2, for a boundary equilibrium $E_2 = (\tilde{s}_1, 0, \tilde{s}_2, \tilde{x}_2)$ we have $(\tilde{s}_1, \tilde{s}_2) = \mathrm{FSB}_1 \cap \mathrm{ZNGI}_2$. This condition is equivalent to

$$\tilde{s}_1 = s_1^{in} \quad \text{and} \quad f_2(\tilde{s}_1, \tilde{s}_2) = D_2. \tag{D.13}$$

The first formula in (D.13) is the first formula in (D.6). Replacing $\tilde{s}_1$ in the second formula of (D.13) we have $f_2(s_1^{in}, \tilde{s}_2) = D_2$. Therefore, using Definition 1 we have $\tilde{s}_2 = \lambda_2\left(s_1^{in}, D_2\right)$, which proves the second formula in (D.6). The x_2 component is given then by (3.1), which proves the third formula in (D.6). E_2 exists if and only if equation $f_2\left(s_1^{in}, s_2\right) = D_2$ has a solution in the interval $\left(0, s_2^{in}\right)$. Since $f_2\left(s_1^{in}, 0\right) = 0$, the solution exists if and only if $f_2\left(s_1^{in}, s_2^{in}\right) > D_2$, which proves (D.7).

Using Lemma 2, for $E_c = (s_1^*, x_1^*, s_2^*, x_2^*)$ we have $(s_1^*, s_2^*) \in \mathrm{ZNGI}_1 \cap \mathrm{ZNGI}_2 \cap \mathcal{F}^o$. This condition is equivalent to

$$f_1(s_1^*, s_2^*) = D_1, \quad f_2(s_1^*, s_2^*) = D_2 \quad \text{and} \quad (s_1^*, s_2^*) \in \mathcal{F}^o.$$

Therefore (s_1^*, s_2^*) is a solution of (D.9), lying in the interior $\mathcal{F}^o$ of the feasible set. The x_1 and x_2 components are given then by (3.1), which proves (D.10).

This ends the proof of the existence conditions in the proposition. The local stability of an equilibrium point of (2.5) depends on the sign of the real parts of the eigenvalues of the corresponding Jacobian matrix for the system (2.5). The Jacobian matrix is the matrix of the partial derivatives of the right-hand side the system (2.5), with respect to the state variables, evaluated at the given equilibrium point (x_1, x_2, s_1, s_2):

$$J = \begin{bmatrix} f_1 - D_1 & 0 & f_{11}x_1 & f_{12}x_1 \\ 0 & f_2 - D_2 & f_{21}x_2 & f_{22}x_2 \\ -f_1 & 0 & -D - f_{11}x_1 & -f_{12}x_1 \\ f_1 & -f_2 & f_{11}x_1 - f_{21}x_2 & -D + f_{12}x_1 - f_{22}x_2 \end{bmatrix}, \tag{D.14}$$

where f_i and $f_{ij} = \frac{\partial f_i}{\partial s_j}$ are evaluated at the components of the equilibrium point.

At E_0, $x_1 = 0$ and $x_1 = 0$. Hence, the Jacobian matrix (D.14) becomes

$$J_0 = \begin{bmatrix} f_1\left(s_1^{in}, s_2^{in}\right) - D_1 & 0 & 0 & 0 \\ 0 & f_2\left(s_1^{in}, s_2^{in}\right) - D_2 & 0 & 0 \\ -f_1\left(s_1^{in}, s_2^{in}\right) & 0 & -D & 0 \\ f_1\left(s_1^{in}, s_2^{in}\right) & -f_2\left(s_1^{in}, s_2^{in}\right) & 0 & -D \end{bmatrix}.$$

Its eigenvalues are $f_1\left(s_1^{in}, s_2^{in}\right) - D_1$, $f_2\left(s_1^{in}, s_2^{in}\right) - D_2$ and $-D$. Therefore, E_0 is stable if and only if $f_1\left(s_1^{in}, s_2^{in}\right) < D_1$ and $f_2\left(s_1^{in}, s_2^{in}\right) < D_2$ which proves (D.1).

At E_1, $x_2 = 0$ and $x_1 > 0$, so that $f_1 = D_1$. Evaluated at E_1, the Jacobian matrix (D.14) becomes:

$$J_1 = \begin{bmatrix} 0 & 0 & f_{11}(\bar{s}_1, \bar{s}_2)\, x_1 & f_{12}(\bar{s}_1, \bar{s}_2)\, x_1 \\ 0 & f_2(\bar{s}_1, \bar{s}_2) - D_2 & 0 & 0 \\ -D_1 & 0 & -D - f_{11}(\bar{s}_1, \bar{s}_2)\, x_1 & -f_{12}(\bar{s}_1, \bar{s}_2)\, x_1 \\ D_1 & -f_2(\bar{s}_1, \bar{s}_2) & f_{11}(\bar{s}_1, \bar{s}_2)\, x_1 & -D + f_{12}(\bar{s}_1, \bar{s}_2)\, x_1 \end{bmatrix}.$$

Its characteristic polynomial is:

$$P_1(\lambda) = (\lambda + D)\,(\lambda - f_2(\bar{s}_1, \bar{s}_2) + D_2)\left(\lambda^2 + c_1\lambda + c_2\right),$$

where $c_1 = D + (f_{11} - f_{12})(\bar{s}_1, \bar{s}_2)\, x_1$ and $c_2 = D_1(f_{11} - f_{12})(\bar{s}_1, \bar{s}_2)\, x_1$. The eigenvalues of J_1 are $-D$ and $f_2(\bar{s}_1, \bar{s}_2) - D_2$, together with the roots of the quadratic polynomial in $P_1(\lambda)$. Since $f_{11} > 0$ and $f_{12} \leq 0$, one has $c_1 > 0$ and $c_2 > 0$. Hence, the roots of the quadratic polynomial have negative real parts. Therefore, E_1 is stable if and only if $f_2(\bar{s}_1, \bar{s}_2) < D_2$, which proves (D.5).

At E_2, $x_1 = 0$ and $x_2 > 0$, so that $f_2 = D_2$. Evaluated at E_2, the Jacobian matrix (D.14) becomes:

$$J_2 = \begin{bmatrix} f_1(\tilde{s}_1, \tilde{s}_2) - D_1 & 0 & 0 & 0 \\ 0 & 0 & f_{21}(\tilde{s}_1, \tilde{s}_2)\, x_2 & f_{22}(\tilde{s}_1, \tilde{s}_2)\, x_2 \\ -f_1(\tilde{s}_1, \tilde{s}_2) & 0 & -D & 0 \\ f_1(\tilde{s}_1, \tilde{s}_2) & -D_2 & -f_{21}(\tilde{s}_1, \tilde{s}_2)\, x_2 & -D - f_{22}(\tilde{s}_1, \tilde{s}_2)\, x_2 \end{bmatrix}.$$

Its characteristic polynomial is:

$$P_2(\lambda) = (\lambda + D)\,(\lambda - f_1(\tilde{s}_1, \tilde{s}_2) + D_1)\left(\lambda^2 + c_1\lambda + c_2\right),$$

where $c_1 = D + f_{22}(\tilde{s}_1, \tilde{s}_2)\, x_2$ and $c_2 = D_2 f_{22}(\tilde{s}_1, \tilde{s}_2)\, x_2$. The eigenvalues of J_2 are $-D$ and $f_1(\tilde{s}_1, \tilde{s}_2) - D_1$, together with the roots of the quadratic polynomial in $P_2(\lambda)$. Since $f_{22} > 0$, one has $c_1 > 0$ and $c_2 > 0$. Hence, the roots of the quadratic polynomial have negative real parts. Therefore, E_2 is stable if and only if $f_1(\tilde{s}_1, \tilde{s}_2) < D_1$, which proves (D.8).

At E_c, $x_1 > 0$ and $x_2 > 0$, so that $f_1 = D_1$ and $f_2 = D_2$. Evaluated at E_c, the Jacobian matrix (D.14) becomes:

$$J_c = \begin{bmatrix} 0 & 0 & f_{11}x_1 & f_{12}x_1 \\ 0 & 0 & f_{21}x_2 & f_{22}x_2 \\ -D_1 & 0 & -D - f_{11}x_1 & -f_{12}x_1 \\ D_1 & -D_2 & f_{11}x_1 - f_{21}x_2 & -D + f_{12}x_1 - f_{22}x_2 \end{bmatrix},$$

where f_i and f_{ij} are evaluated at $\left(s_1^*, s_2^*\right)$. Its characteristic polynomial is:

$$P_c(\lambda) = \lambda^4 + c_1\lambda^3 + c_2\lambda^2 + c_3\lambda + c_4,$$

where

$$\begin{aligned}
c_1 &= 2D + (f_{11} - f_{12})x_1 + f_{22}x_2, \\
c_2 &= D^2 + (D + D_1)(f_{11} - f_{12})x_1 + (D + D_2)f_{22}x_2 + (f_{11}f_{22} - f_{12}f_{21})x_1x_2, \\
c_3 &= DD_1(f_{11} - f_{12})x_1 + DD_2f_{22}x_2 + (D_1 + D_2)(f_{11}f_{22} - f_{12}f_{21})x_1x_2, \\
c_4 &= D_1D_2(f_{11}f_{22} - f_{12}f_{21})x_1x_2.
\end{aligned}$$

The eigenvalues are of J_c have negative real parts if and only if the Routh-Hurwitz conditions

$$c_1 > 0, \quad c_3 > 0, \quad c_4 > 0 \quad \text{and} \quad r_1 = c_1c_2c_3 - c_1^2c_4 - c_3^2 > 0, \tag{D.15}$$

are satisfied. We use the following notations

$$A = f_{22}, \qquad B = \frac{f_{11}f_{22} - f_{12}f_{21}}{f_{22}}, \qquad C = \frac{f_{12}(f_{21} - f_{22})}{f_{22}}.$$

Using (3.9) and (3.10), we have $A > 0$, $C \geq 0$ and $B + C = f_{11} - f_{12} > 0$. The coefficients c_i can be written as follows

$$\begin{aligned}
c_1 &= 2D + (B + C)x_1 + Ax_2, \\
c_2 &= D^2 + (D + D_1)(B + C)x_1 + (D + D_2)Ax_2 + ABx_1x_2, \\
c_3 &= DD_1(B + C)x_1 + DD_2Ax_2 + (D_1 + D_2)ABx_1x_2, \\
c_4 &= D_1D_2ABx_1x_2.
\end{aligned}$$

Note that $c_1 > 0$. The condition $c_4 > 0$ is equivalent to $B > 0$. If $B > 0$ then we have $c_3 > 0$. Straightforward computations show that r_1 can be written $r_1 = pq + r$, where

$$p = (D_1Bx_1 - D_2Ax_2)^2, \qquad q = D^2 + D(Bx_1 + Ax_2) + ABx_1x_2,$$

and

$$\begin{aligned}
r =\ & A^2B^2(B + C)(D_1 + D_2)x_1^3x_2^2 + A^3B^2(D_1 + D_2)x_1^2x_2^3 \\
&+AB(D(2D_1 + D_2)(B + C)^2 + CD_1^2(2B + C))x_1^3x_2 \\
&+A^2B(D(D_1 + D_2)(5B + 3C) + C(D_1^2 + D_2^2))x_1^2x_2^2 \\
&+A^3BD(D_1 + 2D_2)x_1x_2^3 + DD_1(D(B + C)^3 + D_1(C^3 + 3BC^2 + 3B^2C))x_1^3 \\
&+AD((B+C)((7D_1+4D_2)B+C(2D_1+D_2))D+CD_1((D_1+2D_2)C+2BD_1))x_1^2x_2 \\
&+A^2D(D(B(4D_1 + 7D_2) + C(D_1 + 2D_2)) + CD_2(2D_1 + D_2))x_1x_2^2 \\
&+A^3D^2D_2x_2^3 + D^2D_1(3D(B + C)^2 + D_1C(2 + C))x_1^2 + 3D^3A^2D_2x_2^2 \\
&+AD^2(D(D_1+D_2)(5B+3C) + 2CD_1D_2)x_1x_2 + 2D^4D_1(B+C)x_1 + 2D^4AD_2x_2.
\end{aligned}$$

Hence, $r_1 > 0$ if $B > 0$. Therefore, the conditions (D.15) are satisfied if and only if $B > 0$, which is equivalent to $(f_{11}f_{22} - f_{12}f_{21})\left(s_1^*, s_2^*\right) > 0$. This proves (D.11). □

Table 9: Conditions of existence and stability of the equilibria of (2.5).

	Existence condition	Stability condition (local)
E_0	Always exists	$f_1\left(s_1^{in}, s_2^{in}\right) < D_1$ and $f_2\left(s_1^{in}, s_2^{in}\right) < D_2$
E_1	$f_1\left(s_1^{in}, s_2^{in}\right) > D_1$	$f_2\left(\bar{s}_1, \bar{s}_2\right) < D_2$
E_2	$f_2\left(s_1^{in}, s_2^{in}\right) > D_2$	$f_1\left(\tilde{s}_1, \tilde{s}_2\right) < D_1$
E_c	$\left(s_1^*, s_2^*\right) \in \mathcal{F}^o$	$(f_{11}f_{22} - f_{12}f_{21})\left(s_1^*, s_2^*\right) > 0$

The conditions of existence and stability of equilibria are summarized in Table 9. Let us prove now Proposition 3.

Proof of Proposition 3. The conditions $f_1\left(s_1^{in}, s_2^{in}\right) < D_1$ and $f_1\left(s_1^{in}, s_2^{in}\right) < D_2$ of stability of E_0 are equivalent to $E_0 \in R_1^- \cap R_2^-$. The condition $f_1\left(s_1^{in}, s_2^{in}\right) > D_1$ of existence of E_1 is equivalent to $E_0 \in R_1^+$. Its condition $f_2(\bar{s}_1, \bar{s}_2) < D_2$ of stability is equivalent to $E_1 \in R_2^-$. The condition $f_2\left(s_1^{in}, s_2^{in}\right) > D_2$ of existence of E_2 is equivalent to $E_0 \in R_2^+$. Its condition $f_1(\tilde{s}_1, \tilde{s}_2) < D_1$ of stability is equivalent to $E_2 \in R_1^-$. The condition of existence of E_c is $\left(s_1^*, s_2^*\right) \in \mathcal{F}^o$. Using $\partial\lambda_1/\partial s_2 = -f_{12}/f_{11}$ and $\partial\lambda_2/\partial s_1 = -f_{21}/f_{22}$, the condition $(f_{11}f_{22} - f_{12}f_{21})\left(s_1^*, s_2^*\right) > 0$ of stability of E_c is equivalent to

$$\frac{\partial\lambda_1}{\partial s_2}\left(s_1^*, s_2^*\right)\frac{\partial\lambda_2}{\partial s_1}\left(s_1^*, s_2^*\right) < 1.$$

This condition means that the signed angle between between the tangent of ZNGI_1 and the tangent of ZNGI_2, at the point of intersection $\left(s_1^*, s_2^*\right)$, is negative. □

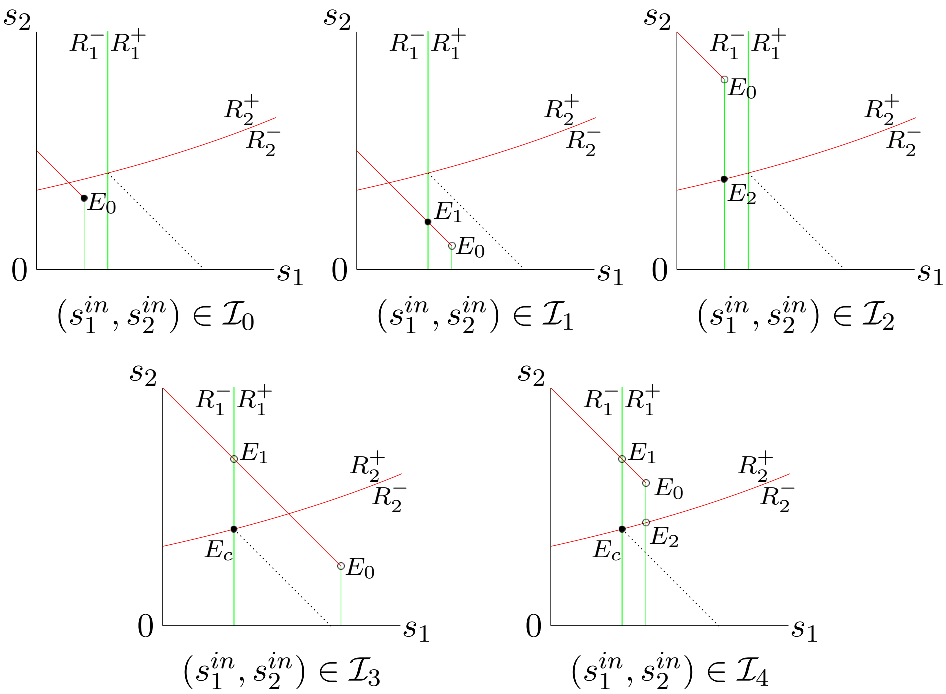

Figure 20: Proof of Proposition 4 in case C2: feasible sets and ZNGIs, showing equilibria and their stability, for the five regions of the operating diagram, shown in Fig. 4 (Case C2).

D.2 Proof of Proposition 4 (Case C2)

The proof is given in Fig. 20. Assume that $\left(s_1^{in}, s_2^{in}\right) \in \mathcal{I}_4$. We see in Fig. 20 that E_0 is unstable, since $E_0 \notin R_1^- \cap R_2^-$, E_1 exists, since $E_0 \in R_1^+$ and is unstable, since $E_1 \notin R_2^-$, E_2 exists, since $E_0 \in R_2^+$ and is unstable since $E_2 \notin R_1^-$, and E_c exists, is unique and stable since, at E_c, $(\text{ZNGI}_1, \text{ZNGI}_2) < 0$. The proof for global asymptotic stability is given in Section B.1. This proves the results depicted in the last row of Table 2. The proofs for the other regions are illustrated in Fig. 20.

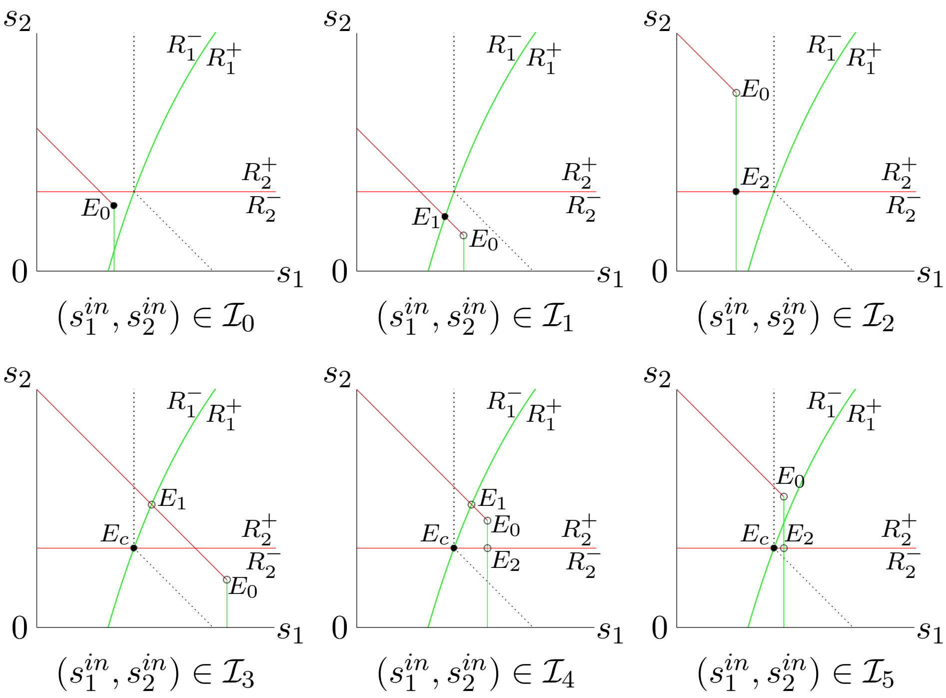

Figure 21: Proof of Proposition 5: feasible sets and ZNGIs, showing equilibria and their stability, for the six regions of the operating diagram, shown in Fig. 4 (Case S1).

D.3 Proof of Proposition 5

The proof is given in Fig. 21. Assume that $\left(s_1^{in}, s_2^{in}\right) \in \mathcal{I}_5$. We see in Fig. 21 that E_0 is unstable since $E_0 \notin R_1^- \cap R_2^-$, E_1 does not exist, since $E_0 \notin R_1^+$, E_2 exists, since $E_0 \in R_2^+$, and is unstable, since $E_2 \notin R_1^-$, and E_c exists, is unique and stable since, at E_c, $(\text{ZNGI}_1, \text{ZNGI}_2) < 0$. This proves the results depicted in the last row of Table 3. The proofs for the other regions are illustrated in Fig. 21. When $D_1 = D_2 = D$, the proof for global asymptotic stability is given in Section B.2.

D.4 Proof of Proposition 8 ($\mathcal{I}_k$ regions, $k = 0, \ldots, 8$)

The proof is given in Fig. 22. Assume that $(s_1^{in}, s_2^{in}) \in \mathcal{I}_8$. We see in Fig. 22 that E_0 is unstable since $E_0 \notin R_1^- \cap R_2^-$, E_1 exists since $E_0 \in R_1^+$ and is stable since $E_1 \in R_2^-$, E_2^1 and E_2^2 exist since $E_0 \in R_{22}^-$ and E_2^1 is unstable since $E_2^1 \notin R_1^-$, E_c^1 and E_c^2 exist. The proofs for all other regions are similar.

E Review of models of commensalism and syntrophy

In this section we review the main results of the existing literature concerning the systems described in Figs. 1 and 10 and briefly summarize their contributions.

Table 10 presents the main studies of the commensalistic models C1 and C2, while Table 11 presents the studies for the syntrophic models S1 and S2. The studies for the model including sel-inhibition are presented in Tables 12 and 13. The growth functions used in these tables are defined in Table 14. For details and complements the reader can consult the review paper [54] and [20, 40].

To our knowledge, Reilly [36] was the first to propose a mathematical study of the pure commensalistic

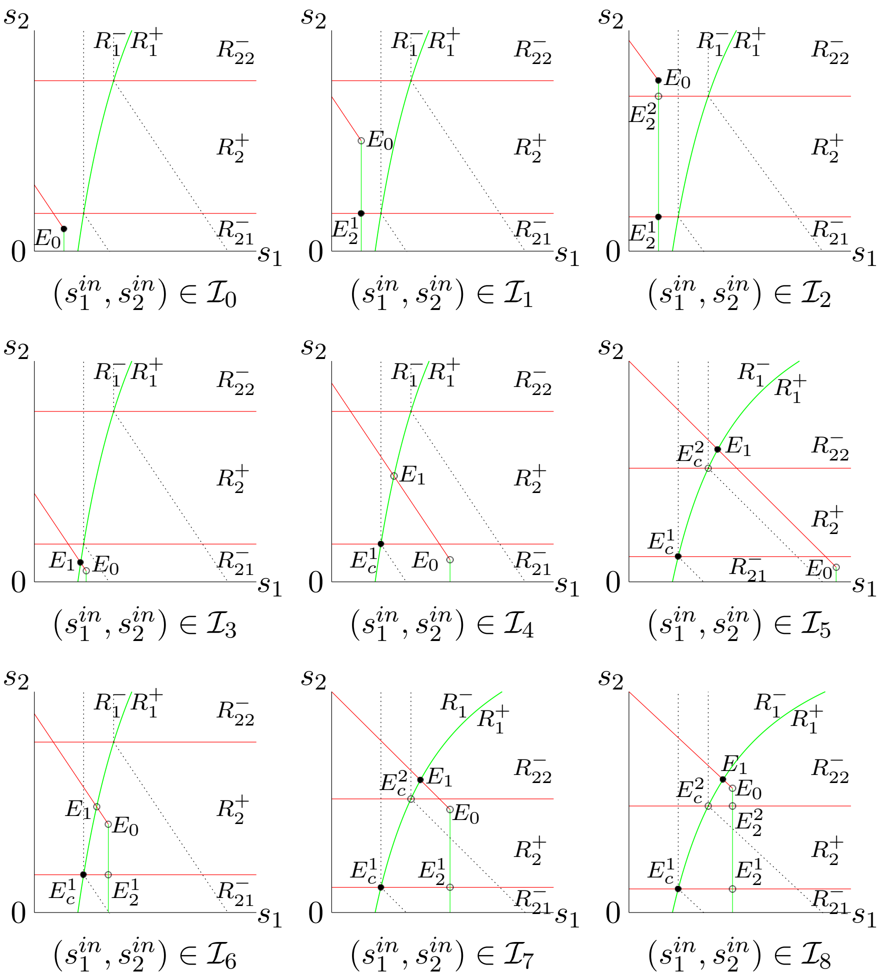

Figure 22: Proof of Proposition 8: feasible sets and ZNGIs, showing equilibria and their stability, for the nine regions of the operating diagram, shown in Fig.12 (Case S1_2).

model C1, with Monod growth functions and without decay terms of the species. He also considered more complicated commensalistic systems when feedback inhibition and feedforward activation occur, to explain oscillations observed in experimental data.

The work of Stephanopoulos [47], is an important contribution to commensalism. He considered general growth functions and investigated the case of nonmonotone growth functions. In the case of equal removal rates, he reduced the system to a planar system and gave a complete qualitative description of the cases C1, C1_1, C1_2 and C1_{12}, see Figs. 3 and 4 in [47].

The classical two-step (acidogenesis-methanisation) dynamical representation of anaerobic digestion processes (see equation (1.85) in [5]) has the structure of the pure commensalistic model C1 or its extension C1_2, obtained by adding an inhibition by the second substrate. It was used by Simeonov and Stoyanov [44] for the control of the process who considered C1, with Monod growth functions and including decay terms.

An important contribution to the modelling of anaerobic digestion as the commensalistic system C1_2 is the model of Bernard et al. [9] with a Monod function for μ_1 and a Haldane function for μ_2. Their model, sometimes referred to as AMOCO or AM2, included the term α which represents the fraction of the

Table 10: Models of commensalistic relationship. The growth functions μ_1 and μ_2 are defined in Table 14.

μ_1	μ_2	S_2^{in}	D_i	Year Ref.	Case
Monod	Monod	0	D	1974 Reilly [36]	C1
M-function	M-function	0	D	1981 Stephanopoulos [47]	C1
Monod	Monod	0	$D + a_i$	2003 Simeonov and Stoyanov [44]	C1
Monod	Monod	0	D	2019 Di and Yang [17]	C1
Monod	I-Monod	0	D	2019 Di and Yang [17]	C2
M-function	I-M-function	0	D	2019 Ben Ali [7]	C2

Table 11: Models of syntrophic relationship. The growth functions μ_1 and μ_2 are defined in Table 14.

μ_1	μ_2	S_2^{in}	D_i	Year Ref.	Case
Monod-I	Monod	0	D	1974 Wilkinson et al. [59]	S1
KB1	Monod	0	D	1986 Kreikenbohm and Bohl [28]	S1
M-I-function	M-function	0	D	1994 Burchard [11]	S1
Monod-I	Monod	0	$D + a_i$	2011 Xu et al. [60]	S1
M-I-function	M-function	0	D	2010 El Hajji et al. [18]	S1
M-I-function	M-function	0	$D + a_i$	2016 Sari and Harmand [40]	S1
M-I-function	M-function	≥ 0	$D + a_i$	2018 Daoud et al. [15]	S1
Monod-I	Monod	0	D	2019 Di and Yang [17]	S1
M-I-function	M-function	≥ 0	D	2023 Albargi and El Hajji [2]	S1
M-I-function	I-M-function	0	D	2012 Sari et al. [39]	S2
Monod-I	I-Monod	0	D	2019 Di and Yang [17]	S2

biomass in the liquid phase. Simeonov and Diop [43] studied this model for $\alpha = 1$. Sbarciog et al. [42] and Weedermann [56] studied the model with general growth function and $\alpha = 1$, while the interesting case where $0 < \alpha \leq 1$ was studied by Benyahia et al. [8]. Bayen and Gajardo [6] studied the steady state optimization of the biogas production of AM2, while the operating diagram of the model is described in [38]. For more details and complements on anaerobic digestion, the reader is referred to the recent review [53].

The system S1 with a syntrophic relationship between the species was considered by Wilkinson [59], with an inhibited Monod growth function for μ_1 and a Monod growth function for μ_2, while Kreikenbohm and Bohl [28] considered another form of feedback of the second substrate on the first species, see Table 14. Burchard [11] extended the results of [28, 59] to a large class of general growth functions. He highlighted conditions under which there is persistence or extinction. El Hajji et al. [18], also obtained results for general growth functions. The studies in [11, 18, 28, 59] have shown that, if it exists, the positive coexistence equilibrium is unique and stable, and there is no other stable equilibrium.

All these studies did not include the decay terms of the species. Xu et al. [60] consindred the effects of the decay terms and studied the model S1 with an inhibited Monod growth function for μ_1 and a Monod growth function for μ_2, and $S_2^{in} = 0$. These authors leaved unanswered the question of the stability of the positive steady state as long as it exists. Sari and Harmand [40] considered S1 with general growth functions and proved that the positive steady state is stable whenever it exists. Daoud et al. [15] extended the results of [40], to the case $S_2^{in} > 0$, showing the appearance of a new boundary equilibrium where species X_1 is absent, while species X_2 is present.

The system S1$_2$ which includes in addition an inhibition of the second species by the second substrate was considered by Harvey et al. [24] in the case without decay terms, where $\mu_1(S_1, S_2)$ is the product of an

Table 12: Models of commensalistic relationship with self inhibitions. The growth functions μ_1 and μ_2 are defined in Table 14.

μ_1	μ_2	S_2^{in}	D_i	Year Ref.	Case
H-function	M-function	0	D	1981 Stephanopoulos [47]	$C1_1$
M-function	H-function	0	D	1981 Stephanopoulos [47]	$C1_2$
Monod	Haldane	≥ 0	αD	2001 Bernard et al. [9]	$C1_2$
Monod	Haldane	≥ 0	D	2010 Simeonov and Diop [43]	$C1_2$
M-function	H-function	0	D	2010 Sbarciog et al [42]	$C1_2$
M-function	H-function	≥ 0	αD	2012 Benyahia et al. [8]	$C1_2$
M-function	H-function	0	D	2012 Weedermann [56]	$C1_2$
M-function	H-function	≥ 0	αD	2018 Bayen and Gajardo [6]	$C1_2$
M-function	H-function	≥ 0	αD	2020 Sari and Benyahia [38]	$C1_2$
M-function	H-function	≥ 0	$\alpha_i D + a_i$	2022 Sari [37]	$C1_2$
H-function	H-function	0	D	1981 Stephanopoulos [47]	$C1_{12}$

Table 13: Models of syntrophic relationship with self inhibitions. The growth functions μ_1 and μ_2 are defined in Table 14.

μ_1	μ_2	S_2^{in}	D_i	Year Ref.	Case
KB2	I-Monod	0	D	1988 Kreikenbohm and Bohl [29]	$S2_1$
HGG	H-function	0	D	2014 Harvey et al. [24]	$S1_2$
M-I function	H function	≥ 0	$D + a_i$	2017 Fekih-Salem et al. [19]	$S1_2$
M-I function	H function	≥ 0	$\alpha_i D + a_i$	2020 Fekih-Salem et al. [20]	$S1_2$

increasing function of S_1 and a decreasing function of S_2, which is a particular case of M-I-functions, while $\mu_2(S_2)$ is an H-function, see Fig. 2 in [24]. The more general case of M-I-function, also including decay terms of the species, where the stability analysis is much more delicate since the system cannot be reduced to a planar system, was considered by Fekih-Salem et al. [19, 20].

The system S2, with two inhibitions, was considered by Sari et al. [39] who showed that, in contrast with the case of S1 with only an inhibition of the second substrate on the first species, a multiplicity of positive equilibria can occur.

An example of system $S2_1$ with three different inhibitions was considered by Kreikenbohm and Bohl [29]. The mathematical analysis of this model shows the occurrence of bistability as in the case of the system S2, without the additional inhibition of the first species by its limiting substrate.

Other models for which μ_1 and μ_2 depend both on (S_1, S_2) and, in addition, X_1 and X_2 are in competition on substrate S_1, exhibiting the multiplicity of positive equilibrium points can be found in [52]. An important and interesting extension should be mentioned here: [57] proposed an 8-dimensional mathematical model, which includes syntrophy and inhibition, both mechanisms considered by [9] and by [18]. The effects of decay terms are considered by [58].

Acknowledgements

The author would like to thank Radhouane Fekih-Salem and Claude Lobry for their careful reading, which improved the presentation considerably. The author thanks the TREASURE Euro-Mediterranean research network for partial financial support.

Table 14: Growth functions used in Tables 10, 11, 12 and 13

Function	Definition
Monod	$\mu_i(S_i) = \frac{m_i S_i}{K_i + S_i}$
Monod-I	$\mu_1(S_1, S_2) = \frac{m_1 S_1}{K_1 + S_1} \frac{1}{1 + L_2 S_2}$
I-Monod	$\mu_2(S_1, S_2) = \frac{m_2 S_2}{K_2 + S_2} \frac{1}{1 + L_1 S_1}$
KB1	$\mu_1(S_1, S_2) = \begin{cases} \frac{m_1(S_1 - S_2/K_2)}{K_1 + S_1 + L_1 S_2} & \text{if } S_1 - S_2/K_2 > 0 \\ 0 & \text{otherwise} \end{cases}$
Haldane	$\mu_2(S_2) = \frac{m_2 S_2}{K_2 + S_2 + S_2^2/K_I}$
KB2	$\mu_1(S_1, S_2) = \begin{cases} \frac{m_1(S_1 - S_2/K_2)}{K_1 + S_1 + L_1 S_2 + S_1^2/K_I} & \text{if } S_1 - S_2/K_2 > 0 \\ 0 & \text{otherwise} \end{cases}$
M-function	$\mu(0) = 0$ and for $S > 0$, $\mu'(S) > 0$
H-function	$\mu(0) = 0$ and $\begin{cases} \text{there is } S^m \in (0, +\infty] \text{ such that} \\ \mu'(S) > 0 \text{ for } S < S^m \text{ and } \mu'(S) < 0 \text{ for } S > S^m. \\ \text{(Note that if } S^m = +\infty, \text{ we obtain an M-function).} \end{cases}$
M-I function	$\mu_1(0, S_2) = 0$ and, for $S_1, S_2 > 0$, $\frac{\partial \mu_1}{\partial S_1}(S_1, S_2) > 0$, $\frac{\partial \mu_1}{\partial S_2}(S_1, S_2) \le 0$
I-M function	$\mu_2(S_1, 0) = 0$ and, for $S_1, S_2 > 0$, $\frac{\partial \mu_2}{\partial S_2}(S_1, S_2) > 0$, $\frac{\partial \mu_2}{\partial S_1}(S_1, S_2) \le 0$
HHG	$\mu_1(S_1, S_2) = f(S_1) I(S_2)$ with $\begin{cases} f(0) = 0, f'(S_1) > 0 \text{ for } S_1 > 0 \\ \text{and } I'(S_2) < 0 \text{ for } S_2 > 0. \end{cases}$

References

[1] N. Abdellatif, R. Fekih-Salem and T. Sari, Competition for a single resource and coexistence of several species in the chemostat, *Math. Biosci. Eng.* 13 (2016) 631–652. `http://dx.doi.org/10.3934/mbe.2016012`

[2] A.H. Albargi and M. El Hajji, Mathematical analysis of a two-tiered microbial food-web model for the anaerobic digestion process. *Math. Biosci. Eng.*, 20 (2023) 6591–6611. `http://dx.doi.org/10.3934/mbe.2023283`

[3] M.M. Ballyk and G.S.K. Wolkowicz, Classical and resource-based competition: a unifying graphical approach, *J. Math. Biol.* 62 (2011) 81–109. `http://dx.doi.org/10.1007/s00285-010-0328-x`

[4] B. Bar and T. Sari, The operating diagram for a model of competition in a chemostat with an external lethal inhibitor. *Discrete Contin. Dyn. Syst. B* 25 (2020) 2093–2120. `http://dx.doi.org/10.3934/dcdsb.2019203`

[5] G. Bastin and D. Dochain, *On-line Estimation and Adaptive Control of Bioreactors*, Process Measurement and Control. Elsevier (1990).

[6] T. Bayen and P. Gajardo, On the steady state optimization of the biogas production in a two-stage anaerobic digestion model. *J. Math. Biol.* 78 (2019) 1067–1087. `http://dx.doi.org/10.1007/s00285-018-1301-3`

[7] N. Ben Ali, Analyse mathématique de la stabilité d'une communauté microbienne synthétique. *Mémoire de Mastère de Recherche*. École Nationale d'Ingénieurs de Tunis, Université de Tunis El Manar, 2019.

[8] B. Benyahia, T. Sari, B. Cherki and J. Harmand, Bifurcation and stability analysis of a two step model for monitoring anaerobic digestion processes. *J. Process Control*, 22 (2012) 1008–1019. http://dx.doi.org/10.1016/j.jprocont.2012.04.012

[9] O. Bernard, Z. Hadj-Sadock, D. Dochain, A. Genovesi and J.P. Steyer, Dynamical model development and parameter identification for an anaerobic wastewater treatment process. *Biotechnol Bioeng.* 75 (2001) 424–438. http://dx.doi.org/10.1002/bit.10036

[10] A. Bornhöft, R. Hanke-Rauschenbach and K. Sundmacher, Steady-state analysis of the anaerobic digestion model no. 1 (ADM1). *Nonlinear Dyn.* 73 (2013) 535–549. http://dx.doi.org/10.1007/s11071-013-0807-x

[11] A. Burchard, Substrate degradation by a mutualistic association of two species in the chemostat, *J. Math. Bio.*, 32 (1994) 465–489. http://dx.doi.org/10.1007/BF00160169

[12] M. Dali-Youcef, A. Rapaport and T. Sari, Study of performance criteria of serial configuration of two chemostats, *Math. Biosci. Eng.* 17 (2020) 6278–6309. http://dx.doi.org/10.3934/mbe.2020332

[13] M. Dali-Youcef, A. Rapaport and T. Sari, Performance study of two serial interconnected chemostats with mortality, *Bull. Math. Biol.* 84 (2022) 110. http://dx.doi.org/10.1007/s11538-022-01068-6

[14] M. Dali-Youcef and T. Sari, The productivity of two serial chemostats, *Int. J. Biomath.* 16 6 (2023) 2250113. http://dx.doi.org/10.1142/S1793524522501133

[15] Y. Daoud, N. Abdellatif, T. Sari and J. Harmand, Steady state analysis of a syntrophic model: The effect of a new input substrate concentration, *Math. Model. Nat. Phenom.*, 13 (2018) 31. http://dx.doi.org/10.1051/mmnp/2018037

[16] M. Dellal, M. Lakrib and T. Sari, The operating diagram of a model of two competitors in a chemostat with an external inhibitor, *Math. Biosci.* 302 (2018) 27–45. http://dx.doi.org/10.1016/j.mbs.2018.05.004

[17] S. Di and A. Yang, Analysis of productivity and stability of synthetic microbial communities. *J. R. Soc. Interface* 16 (2019) 20180859. http://dx.doi.org/10.1098/rsif.2018.0859

[18] M. El Hajji, F. Mazenc and J. Harmand, A mathematical study of a syntrophic relationship of a model of anaerobic digestion process, *Math. Biosci. Eng.*, 7 (2010) 641–656. http://dx.doi.org/10.3934/mbe.2010.7.641

[19] R. Fekih-Salem, N. Abdellatif and A. Yahmadi, Effect of inhibition on a syntrophic relationship model in the anaerobic digestion process, Proceedings of the 8th conference on Trends in Applied Mathematics in Tunisia, Algeria, Morocco, 2017, 391–396, https://indico.math.cnrs.fr/event/1335

[20] R. Fekih-Salem, Y. Daoud, N. Abdellatif and T. Sari, A mathematical model of anaerobic digestion with syntrophic relationship, substrate inhibition and distinct removal rates, *SIAM J. Appl. Dyn. Syst.* 20 (2021) 621–1654. http://dx.doi.org/10.1137/20M137648

[21] R. Fekih-Salem, C. Lobry and T. Sari, A density-dependent model of competition for one resource in the chemostat. *Math. Biosci.* 286 (2017) 104–122. http://dx.doi.org/10.1016/j.mbs.2017.02.007

[22] T. Großkopf and O.S. Soyer, Synthetic microbial communities. *Curr. Opin. Microbiol.* 18 (2014), 72–77. http://dx.doi.org/10.1016/j.mib.2014.02.002

[23] J. Harmand, C. Lobry, A. Rapaport and T. Sari, *The Chemostat: Mathematical Theory of Microorganism Cultures*, Wiley ISTE Editions, 2017.

[24] E. Harvey and J. Heys and T. Gedeon, Quantifying the effects of the division of labor in metabolic pathways, *J. Theor. Biol.*, 360 (2014) 222–242 http://dx.doi.org/10.1016/j.jtbi.2014.07.011

[25] S.G. Hays, W.G. Patrick, M. Ziesack, N. Oxman and P.A. Silver, Better together: engineering and application of microbial symbioses. *Curr. Opin. Biotechnol.* 36 (2015) 40–49. http://dx.doi.org/10.1016/j.copbio.2015.08.008

[26] J. Jost, J. Drake, A. Fredrickson and H. Tsuchiya, Interactions of *Tetrahymena pyriformis*, *Escherichia coli*, *Azotobacter Vinelandii*, and glucose in a minimal medium. *J. Bacteriol.* 113 (1973) 834–840. http://dx.doi.org/10.1128/jb.113.2.834-840.1973

[27] Z. Khedim, B. Benyahia, B. Cherki, T. Sari and J. Harmand, Effect of control parameters on biogas production during the anaerobic digestion of protein-rich substrates. *Appl. Math. Model.* 61 (2018) 351–376. http://dx.doi.org/10.1016/j.apm.2018.04.020

[28] R. Kreikenbohm and E. Bohl, A mathematical model of syntrophic cocultures in the chemostat, *FEMS Microbiol. Ecol.*, 38 (1986) 131–140 http://dx.doi.org/10.1111/j.1574-6968.1986.tb01722.x

[29] R. Kreikenbohm, E. Bohl, Bistability in the Chemostat. it Ecological Modelling 43 (1988) 287–301. http://dx.doi.org/10.1016/0304-3800(88)90009-9

[30] R. E. Lenski and S. E. Hattingh, Coexistence of two competitors on one resource and one inhibitor: A chemostat model based on bacteria and antibiotics, *J. Theoretical Biology* 122 (1986) 83–93. http://dx.doi.org/10.1016/S0022-5193(86)80226-0

[31] J. Monod, La technique de culture continue. Théorie et applications, *Annales de l'Institut Pasteur*, 79 (1950) 390–410. http://dx.doi.org/10.1016/B978-0-12-460482-7.50023-3

[32] T. Mtar, R. Fekih-Salem and T. Sari, Interspecific density-dependent model of predator–prey relationship in the chemostat, *Inter. J. Biomath.* 14 (2021) 2050086. http://dx.doi.org/10.1142/S1793524520500862

[33] T. Mtar, R. Fekih-Salem and T. Sari, Mortality can produce limit cycles in density-dependent models with a predator-prey relationship, *Discrete Contin. Dyn. Syst. B* 27 (2022) 7445–7467. http://dx.doi.org/10.3934/dcdsb.2022049

[34] S. Nouaoura, R. Fekih-Salem, N. Abdellatif and T. Sari, Operating diagrams for a three-tiered microbial food web in the chemostat, *J. Math. Biol.* 85 44 (2022). http://dx.doi.org/10.1007/s00285-022-01812-5

[35] S. Pavlou, Computing operating diagrams of bioreactors, *J. Biotechnol.* 71 (1999) 7–16. http://dx.doi.org/10.1016/s0168-1656(99)00011-5

[36] P.J. Reilly, Stability of commensalistic systems, *Biotechnology and Bioengineering* 16 (1974) 1373–1392. http://dx.doi.org/10.1002/bit.260161006

[37] T. Sari, Best operating conditions for biogas production in some simple anaerobic digestion models. *Processes* 2022 10(2), 258. http://dx.doi.org/10.3390/pr10020258

[38] T. Sari, B. Benyahia, The operating diagram for a two-step anaerobic digestion model, *Nonlinear Dyn.* 105 (2021) 2711–2737. http://dx.doi.org/10.1007/s11071-021-06722-7

[39] T. Sari, M. El-Hajji and J. Harmand, The mathematical analysis of a syntrophic relationship between two microbial species in a chemostat, *Math. Biosci. Eng.*, 9 (2012) 627–645. http://dx.doi.org/10.3934/mbe.2012.9.627

[40] T. Sari and J. Harmand, A model of a syntrophic relationship between two microbial species in a chemostat including maintenance. *Math. Biosci.*, 275 (2016) 1–9. http://dx.doi.org/10.1016/j.mbs.2016.02.008

[41] T. Sari and M. J. Wade, Generalised approach to modelling a three-tiered microbial food-web, *Mathematical Biosciences* 291 (2017) 21–37. http://dx.doi.org/10.1016/j.mbs.2017.07.005

[42] M. Sbarciog, M. Loccufier and E. Noldus. Determination of appropriate operating strategies for anaerobic digestion systems. *Bioch. Eng. J.*, 51 (2010) 180–188. http://dx.doi.org/10.1016/j.bej.2010.06.016

[43] I. Simeonov and S. Diop, Stability analysis of some nonlinear anaerobic digestion models, *Int. J. Bioautomation*, 14 (2010) 37–48. https://hal.archives-ouvertes.fr/hal-00544138

[44] I. Simeonov and S. Stoyanov, Modelling and dynamic compensator control of the anaerobic digestion of organic wastes, *Chem. Biochem. Eng. Q.*, 17 (2003) 285–292. http://silverstripe.fkit.hr/cabeq/past-issues/article/596

[45] H.L. Smith and P. Waltman, *The theory of the chemostat: Dynamics of microbial competition*, Cambridge University Press, 1995.

[46] H. Song, M.Z. Ding, X.O. Jia, Q. Ma and Y.J. Yuan. Synthetic microbial consortia: from systematic analysis to construction and applications. *Chem. Soc. Rev.* 43 (2014) 6954–6981. http://dx.doi.org/10.1039/C4CS00114A

[47] G. Stephanopoulos, The dynamic of commensalism, *Biotechnology and Bioengineering* 23 (1981) 2243–2255. http://dx.doi.org/10.1002/bit.260231008

[48] H. R. Thieme, *Convergence results and a Poincaré-Bendixson trichotomy for asymptotically autonomous differential equations*, *J. Math. Biol.*, 30 (1992) 755–763. http://dx.doi.org/10.1007/BF00173267

[49] H.R. Thieme, Asymptotically autonomous differential equations in the plane, *Rocky Mountain Journal of Mathematics* 24 (1993) 351–380. http://dx.doi.org/10.1216/rmjm/1181072470

[50] D. Tilman, Resources: a graphical-mechanistic approach to competition and predation. *American Naturalist* 116 (1980) 362–393. http://dx.doi.org/10.1086/283633

[51] D. Tilman, *Resource competition and community structure*. Princeton University Press, New Jersey (1982).

[52] E.I.P. Volcke, M. Sbarciog, E.J.L. Noldus, B. De Baets and M. Loccufier, Steady-state multiplicity of two-step biological conversion systems with general kinetics. *Math. Biosci.* 228 (2010) 160–170. http://dx.doi.org/10.1016/j.mbs.2010.09.004

[53] M. J. Wade, Not Just Numbers: Mathematical Modelling and Its Contribution to Anaerobic Digestion Processes, *Processes*, 8 (2020) 888. http://dx.doi.org/10.3390/pr8080888

[54] M.J. Wade, J. Harmand, B. Benyahia, T. Bouchez, S. Chaillou, B. Cloez, J.-J. Godon, B. Moussa Boudjemaa, A. Rapaport, T. Sari, R. Arditi and C. Lobry, Perspectives in mathematical modelling for microbial ecology. *Ecological Modelling* 321 (2016) 64–74. http://dx.doi.org/10.1016/j.ecolmodel.2015.11.002

[55] M.J. Wade, R.W. Pattinson, N.G. Parker and J. Dolfing, Emergent behaviour in a chlorophenol-mineralising three-tiered microbial 'food web', *Journal of Theoretical Biology* 389 (2016) 171–186. http://dx.doi.org/10.1016/j.jtbi.2015.10.032

[56] M. Weedermann, Analysis of a model for the effects of an external toxin on anaerobic digestion. *Mathematical biosciences and engineering* 9 (2012) 445-59. http://dx.doi.org/10.3934/mbe.2012.9.445

[57] M. Weedermann, G. Seo and G. Wolkowics, Mathematical Model of Anaerobic Digestion in a Chemostat: Effects of Syntrophy and Inhibition, *Journal of Biological Dynamics* 7 (2013) 59–85. http://dx.doi.org/10.1080/17513758.2012.755573

[58] M. Weedermann, G. Wolkowicz and J. Sasara, Optimal biogas production in a model for anaerobic digestion. *Nonlinear Dyn.* 81 (2015) 1097–1112. http://dx.doi.org/10.1007/s11071-015-2051-z

[59] T. G. Wilkinson, H. H. Topiwala and G. Hamer, Interactions in a Mixed Bacterial Population Growing on Methane in Continuous Culture. *Biotechnol. Bioeng.* 16 (1974) 41–59. http://dx.doi.org/10.1002/bit.260160105

[60] A. Xu, J. Dolfing, T. Curtis, G. Montague and E. Martin, Maintenance affects the stability of a two-tiered microbial 'food chain'?, *J. Theor. Biol.*, 276 (2011) 35–41. http://dx.doi.org/10.1016/j.jtbi.2011.01.026